Application Scopes of Miniaturized MXene-Functionalized Electrospun Nanofibers-Based Electrochemical Energy Devices

Khademolqorani, Sanaz; Banitaba, Seyedeh Nooshin; Gupta, Ashish; Poursharifi, Nazanin; Ghaffari, Ali Akbar; Jadhav, Vijaykumar V; Arifeen, Waqas Ul; Singh, Mandeep; Borah, Munu; Chamanehpour, Elham; Mishra, Yogendra Kumar

Published in:
Small

DOI:
10.1002/smll.202309572

Publication date:
2024

Document version:
Accepted manuscript

Application Scopes of Miniaturized MXene-Functionalized Electrospun Nanofibers-Based Electrochemical Energy Devices

Sanaz Khademolqorani, Seyedeh Nooshin Banitaba, Ashish Gupta, Nazanin Poursharifi, Ali Akbar Ghaffari, Vijaykumar V. Jadhav*, Waqas Ul Arifeen*, Mandeep Singh, Munu Borah, Elham Chamanehpour, Yogendra Kumar Mishra**

N. Poursharifi, Dr. S. Khademolqorani,
Department of Textile Engineering, Isfahan University of Technology, Isfahan 84156-83111, Iran

Dr. S.N. Banitaba
Department of Textile Engineering, Amirkabir University of Technology, Tehran 159163-4311, Iran
Email: nooshin_bt@yahoo.com

Dr. S. Khademolqorani, Dr. S.N. Banitaba
Emerald Experts Laboratory, Isfahan Science and Technology Town, Isfahan, 84156-83111, Iran.

Prof. A. Gupta, Prof. M. Singh
CSIR-National Physical Laboratory, New Delhi, 110012, India

Dr. A.A. Ghaffari
School of Chemistry, College of Science, University of Tehran, 14155 Tehran, Iran

Prof. V.K. Jadhav
Guangdong Provincial Key Laboratory of Materials and Technologies for Energy Conversion, 241 Daxue Road, Shantou, 515063, China

Prof. V.K. Jadhav
Department of Materials Science and Engineering, Technion-Israel Institute of Technology, Haifa, 3200003, Israel

Prof. V.K. Jadhav
Department of Material Science and Engineering, Guangdong Technion Israel Institute of Technology, 241 Daxue Road, Shantou, Guangdong 515063, China
Email: vijaykumar.jadhav@gtiit.edu.cn

Dr. W.U. Arifeen
School of Mechanical Engineering, 280 Daehak-ro, Gyeongsan-si, Gyeongsangbuk-do, 38541, Yeungnam University, South Korea
Email: waqas@ynu.ac.kr

Dr. M. Borah

This is the author manuscript accepted for publication and has undergone full peer review but has not been through the copyediting, typesetting, pagination and proofreading process, which may lead to differences between this version and the Version of Record. Please cite this article as doi: 10.1002/smll.202309572.

Department of Physics, School of Basic Sciences, Kaziranga University, Jorhat 785006, India

E. Chamanehpour
Department of Environmental Engineering, Faculty of Natural Resources and Environment, University of Birjand, Birjand 9717434765, Iran

E. Chamanehpour, Prof. Y.K. Mishra
Mads Clausen Institute, Smart Materials, University of Southern Denmark, Alsion 2, 6400, Sønderborg, Denmark
Email: mishra@mci.sdu.dk

Keywords: Electrospun fibers, Battery, Fuel cell, Biosensor, Supercapacitor, Actuators.

ABSTRACT

Exploring combinatorial materials, as well as rational device configuration design, are assumed to be the key strategies for deploying versatile electrochemical devices. MXene sheets have revealed a high hydrophilic surface with proper mechanical and electrical characteristics, rendering them supreme additive candidates to integrate in electrospun electrochemical power tools. The synergetic effects of MXene 2D layers with the nanofibrous networks could boost actuator responsive ability, battery capacity retention, fuel cell stability, sensor sensitivity, and supercapacitor areal capacitance. Their superior mechanical features could be endowed to the electrospun layers through the embedding of the MXene additive. In this review, the preparation and inherent features of the MXene configurations are briefly evaluated. The fabrication and overall performance of the MXene-loaded nanofibers applicable in electrochemical actuators, batteries, fuel cells, sensors, and supercapacitors are comprehensively figured out. Eventually, an outlook on the future development of MXene-based electrospun composites is presented. A substantial focus has been devoted to date to engineering conjugated MXene and electrospun fibrous frames. The potential performance of the MXene-decorated nanofibers presents a bright future of nanoengineering toward technological growth. Meanwhile, a balance between the pros and cons of the synthesized MXene composite layers is worthwhile to consider in the future.

1. Introduction

The escalating use of fossil fuels has sparked global environmental concerns, driving a shift towards cleaner and sustainable energy alternatives [1]. Renewable energy systems, including lithium batteries, supercapacitors, fuel cells, photocatalysts, and electrocatalysts, are being explored to counter the growing pressures of the energy crisis while mitigating environmental impact [2]. Within this context, advanced catalytic materials, with exceptional strength, energy density, and favorable electrochemical properties, are emerging as promising solutions to address the rising demand for renewable energy sources. These materials play a central role in energy conversion and storage, shaping the trajectory towards sustainability [3]. Simultaneously, graphene and its derivatives exhibit remarkable electrocatalytic properties, opening avenues for high-efficiency electrocatalytic systems. These two-dimensional nanomaterials distinguish themselves through their expansive surface area, superior electrical conductivity, and chemical stability. Researchers, building on graphene's success, are synthesizing two-dimensional (2D) nanomaterials and their derivatives to further enhance electrocatalysis [4].

Following the advent of carbon-based structures, the MXene family has opened a new portal in various applications as a transition metal for carbonitrides or carbides since 2011. MXenes are eligible for their outstanding layered array, great electrical conductivity, appropriate mechanical robustness, proper hydrophilicity, as well as ideal optical and thermal properties [5-7]. MXene, as a new class of additive, modifier, or booster, has been widely utilized in diverse material frames, such as polymer films [8, 9], 3D printed layers [10, 11], electro-written structures [12], electrospun mats [13], and so forth.

Costume-made fibers could be synthesized through different routes, in which electrospinning is known as the most feasible nanofabrication system. Electrospun layers offer merits,

including ultrafine fibrous channels comprising tiny interconnected pores, controlled fiber diameter, biocompatibility, and lightweight [14]. Additionally, a highly porous configuration along with tunable morphology could be approached by using simple equipment [15]. Meanwhile, it still faces several limitations, such as ineffective pore structure control ability, hydrophobic nature, insufficient mechanical features, poor electrical conductivity, distortion, etc. [16-18]. Therefore, tremendous efforts have suggested addressing the aforementioned obstacles through direct embedding of the high-efficient nanoparticles into the electrospun fibers or depositing them on the electrospun fibrous layers [19, 20]. The synergy resulting from the combination of MXene fibers and materials, by creating mechanical, electrical, optical, chemical, thermal and catalytic properties, can meet the specific needs of electrochemical devices and become a powerful tool for their practical application (**Figure 1**).

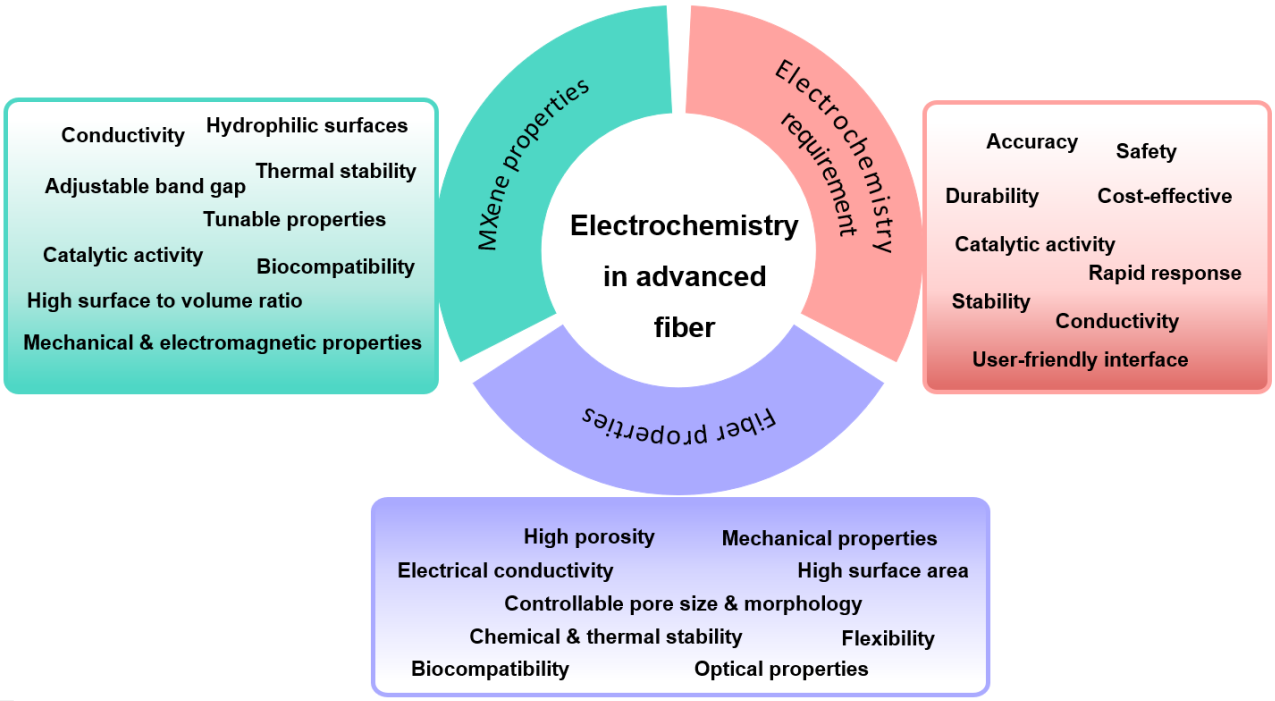

Figure 1. Diverse attributes of fibers, MXenes, and their impact on electrochemical devices requirement.

Simultaneous integration of electrospun architectures with the MXene element has set a research boom in various electrochemical devices. Electrochemical energy storage and conversion could compensate for the shortcoming of global warming, as well as fossil fuels' rapid depletion resulting from ever-increasing energy consumption [21, 22]. Actuators, batteries, fuel cells, sensors, and supercapacitors are customary electrochemical devices, which are being modified day by day [14, 23]. As is apparent in **Figure 2a**, after the MXene discovery by Barsoum and Gogostsi, it was utilized in the PVA electrospun structure for energy storage applications, declaring the conductivity increment up to 0.8 mS cm^{-1} [24]. A PVP-based porous carbon nanofibrous network decorated with MXenes was also introduced by Wang et al. [25] in 2017 as an oxygen reduction reaction electrocatalyst for boosting the functionality of the fuel cells, depicting an onset potential of 0.9 V and a Tafel slope of 60.2 $mV.dec^{-1}$ in the condition of 0.1 M KOH. The MXene was embedded into the PVA nanofibers to fabricate an electrochemical gas sensor with sensing capability in the range of 50 ppb to saturated vapor, as well as a fast response of less than 2 min [26]. In 2019, fibrous carbonized PAN nanofibers were incorporated with MXene nanosheets, representing a capacitance of 205 $mF.cm^{-2}$ in 50 $mV.s^{-1}$ [13]. Guo et al. [27], in another attempt, introduced the PAN-based carbon nanofibers embedded with Fe_3O_4@MXene as the anode component of the lithium secondary batteries with a reversible capacity of 806 mAh g^{-1} at 2 Ag^{-1} after 500 cycles. In 2022, the crystal nanocellulose fibrous mat was integrated with the MXene structure to provide an actuator with the ability to lift 265 times heavier objects in 10 s [28].

Co-occurrences of the most repeated keywords in the published papers from 2015 to 2022, including Mxene, anodes, electrodes, electrolytes, supercapacitors, lithium-ion batteries, biosensors, electrochemical electrodes, energy storage, fuel cell, asymmetric supercapacitor, nanosheet, nanomaterial, electrochemical performance, electrocatalysis, doping, deposition,

and transition metals, relating to the applying MXenes in different electrochemical devices are illustrated in **Figure 2b**. Based on the data obtained, most researches are carried out in the field of battery and supercapacitors. **Figure 2c** also figured out the number of published papers linked with the electrochemical tools formed by the nanofibrous networks, as well as the MXene-loaded electrochemical devices, confirming the results obtained by the VOSviewer. The number of Scopus-indexed publications was also driven, showing a dramatic increment in the research efforts regarding both MXene-based and electrospun electrochemical devices, as shown in **Figures 2d&e**, respectively. Correspondingly, the electrospun frameworks loaded with MXene have opened a new gate for the preparation of versatile electrochemical devices. Based on our knowledge, there is no comprehensive overview evaluating the synergetic effect of MXene nanosheets and electrospun networks as electrochemical devices. Herein, we reviewed the synthesis route, as well as the design of MXene nanostructures, in the following section. Then, the application of MXene in the electrospun electrochemical devices, including actuators, batteries, fuel cells, biosensors, and supercapacitors, was comprehensively figured out. Additionally, the knowledge gap and future perspectives are remarked regarding each application. This review endows a promising opportunity for researchers to explore progressive ideas toward the synthesis of high-performance electrochemical devices.

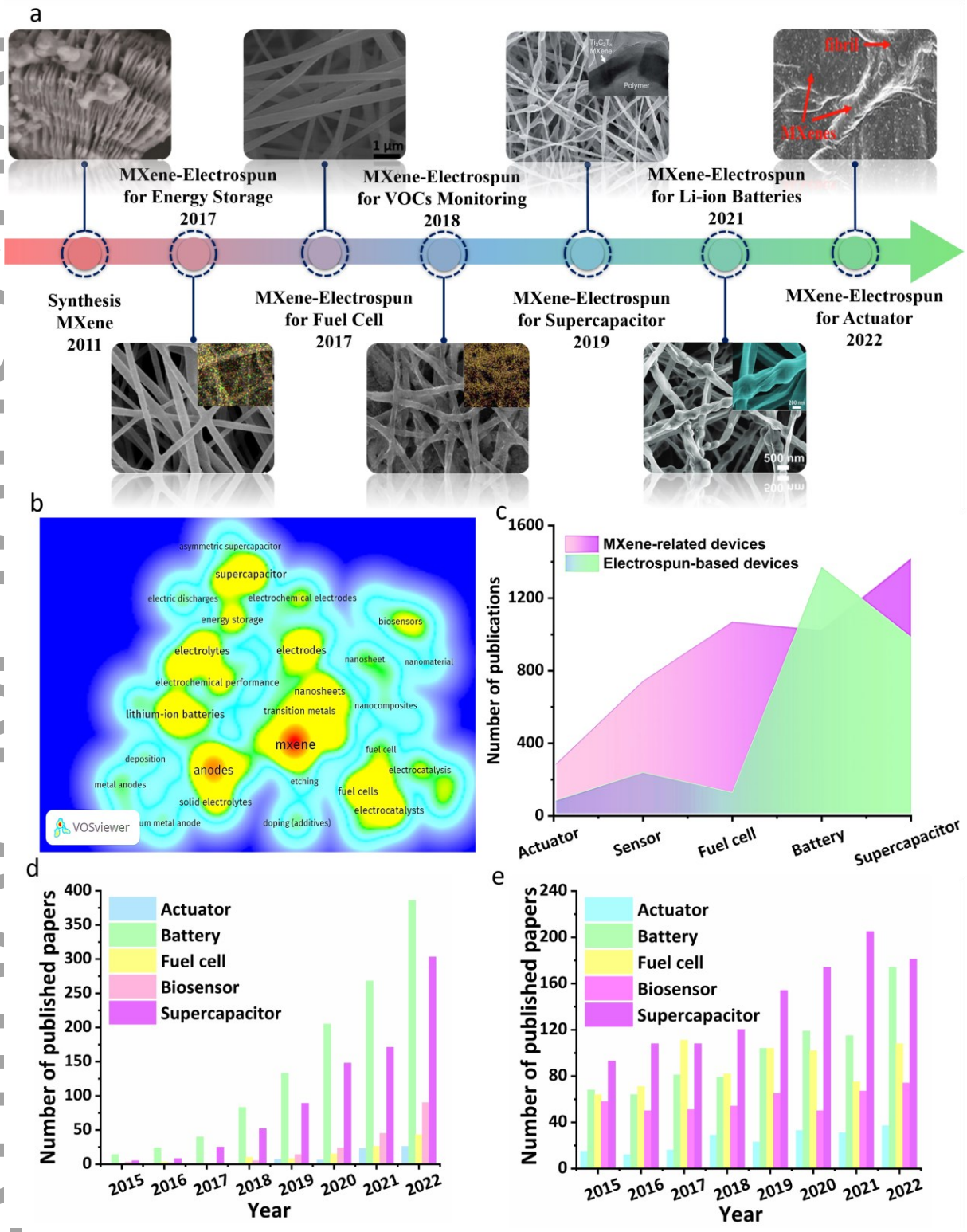

Figure 2. MXene history and application in electrochemical devices; (a) MXene structure, MXene/PVA battery electrodes, MXene/PVA gas sensor, MXene/PAN supercapacitor, and MXene cellulose actuator, respectively, reproduced from references [13, 24-26, 28, 29] with permissions from Wiley, PLOS, Royal society of chemistry, and Elsevier. (b) VOSviewer

bibliometric analysis of keywords related to employing MXene in electrochemical devices, (c) the number of total publications related to electrochemical devices comprising MXene or electrospun fibers, and the number of published papers regarding the application of (d) MXene, and (e) electrospun fibers in the electrochemical devices.

2. MXene structure, properties, and synthesis methods

Recently, the scientific community has been drawn to the remarkable physiochemical properties of two-dimensional (2D) nanomaterials. Since the graphene discovery with exceptional properties in 2004, the range of 2D nanomaterials that have piqued the interest of scientists has significantly expanded [30, 31]. Carbides and nitrides of early transition metals are important materials with broad industrial applications, resulting from revealing outstanding physical and chemical properties [32]. Early transition metallic compositions include metals from groups 3 to 6 of the periodic table, such as zirconium, titanium, hafnium, vanadium, niobium, and tantalum. Among them, carbides and nitrides have high melting points, excellent corrosion resistance, and good mechanical properties, like proper mechanical strength and high hardness. They also have remarkable thermal and electrical conductivity, making them valuable in various applications [32]. These materials are used to make functional composites, materials, and electrochemical energy storage devices. Meanwhile, the process of creating 1D and 2D nanomaterials from 3D solid bulk is challenging because of the strong covalent and metallic bonding between transition metal elements and carbon/nitrogen atoms [33].

MXenes are a type of 2D inorganic compound made up of thin layers comprising nitrides, carbides, and carbonitrides of early transition metals. These materials are named after graphene due to their similar appearance [29, 34]. To create MXenes, layers of the MAX phase are removed via a chemical etching process. The MAX phase is signified by the chemical formulation of

$M_{n+1}AX_n$, where "M" represents transition d-metals (e.g., Ti, Mo, Zr, or Cr), "A" denotes an element from group 13 or 14 (e.g., Al, Ge, Si, or Ga), and "X" signifies carbon and/or nitrogen, with n ranging from 1 to 3 [35, 36]. The MAX phase has a hexagonal construction consisting of densely packed layers with M and X atoms occupying octahedral positions [37]. The first generation of MXenes was created using MAX phases like Ti_2AlC, Nb_2AlC, Ta_4AlC_3, and V_2AlC. Subsequently, the resulting MXenes have the formula $M_{n+1}X_nT_z$ after the selective etching of A layers, where Tz is linked with the surface termination group bonded to M, such as -F, -O, -OH, and so on, and z corresponds to the number of functional groups on its surface [38]. Ti_3C_2 is the most well-known MXene, which is typically produced through the immersion of Ti_3AlC_2 powder in hydrofluoric acid (HF) at ambient temperature [39].

There are several routes to synthesize MXenes, each with pros and cons. The choice of method depends on factors such as scalability, cost, and the favorite characteristics of the resulting MXene. Wet chemical, electrochemical, hydrothermal, and molten salt etching are some of the most common techniques of MXene synthesis [7, 40, 41]. The wet chemical etching method involves the use of a solution containing HF, as well as an intercalating agent, which is employed to expand the interlayer spacing of the MAX phase, facilitating the selective etching of the A layer, and the subsequent delamination of the MXene layers. The intercalating agent could be selected from an extensive range of compounds, including lithium fluoride, urea, and sodium chloride [42, 43].

The etching process involves immersing the MAX phase in the solution for a certain period, typically several hours, at a controlled temperature. The etching solution reacts with the A layer, producing gaseous products and leaving behind the MXene layers. The resulting MXenes could be further treated to modify their features through surface functionalization or thickness adjustment [39]. The resulting MXene layers are typically thin and transparent, making them

appropriate for versatile applications, like energy storage and transparent conductive coatings [36]. Meanwhile, this process could be challenging to scale up, and using HF requires careful handling due to its corrosive nature [44]. Several attempts have been made to minimize or eliminate HF use during wet chemical etching. As an example, Dirscoll and colleagues reduced the amount of HF required by 90% by utilizing the combination of HCl, water, and HF in a 6:3:1 volumetric ratio to synthesize Ti_3C_2 MXene. They also found that the resulting MXene nanosheets had fewer structural defects and could be produced in large sizes with a high yield at ambient temperature [45]. Ghidiu et al. conducted a new tactic to decline the HF content in the etching process of some MAX phases via the combination of LiF and HCl as an alternative to HF, where HF is produced by the LiF and HCl reaction. This approach is known as the Minimally Intensive Layer Delamination (MILD) method, allowing for a one-step etching process and delamination without requiring sonication. The suggested procedure enables laboratories to initiate MXene production at a larger lateral size [46].

Electrochemical etching involves using an electrolytic cell to selectively etch the A component from MAX phases. The process is similar to wet chemical etching, but instead of using HF, the etching is performed using an electric current [47, 48]. This method has the advantage of being more scalable and environmentally friendly than wet chemical etching, but it requires a specialized set-up and could be more challenging to monitor [49]. Sun et al. stated the preparation of Ti_2CT_z and Ti_3C_3Tz through hindering the A elements from Ti_2AlC and Ti_3AlC_2 MAX phases using 2 M HCl, 1 M NH_4Cl, and 0.2 M tetramethylammonium hydroxide as the electrolytes. Meanwhile, excessive etching could lead to the transformation of the MAX phase into carbon as a reason for the simultaneous dissolution of both A and M elements [48].

In the hydrothermal synthesis method, MXenes are synthesized by reacting MAX phases with a hydrothermal solution of alkali metal hydroxide, such as potassium hydroxide (KOH), at high

temperature and pressure [50, 51]. The resulting MXenes are usually thicker and have a higher crystallinity than those obtained by wet chemical or electrochemical etching. This method has the advantage of being more scalable than wet chemical etching and does not require the use of HF. However, it requires high-temperature and high-pressure conditions, which can limit its scalability [52]. Ashraf et al. prepared delaminated-Ti_3C_2/V_2O_5 (d-Ti_3C_2/V_2O_5) nanocomposites using the hydrothermal method for water-splitting applications. They claimed that, in the hydrogen evolution reaction, the prepared hybrid MXene has shown a high rate of activity and might accelerate electron transfer during the procedure of water splitting [50]. The chemical structure and the etching procedures commonly employed for the synthesis of the MXene frameworks are displayed in **Figure 3**.

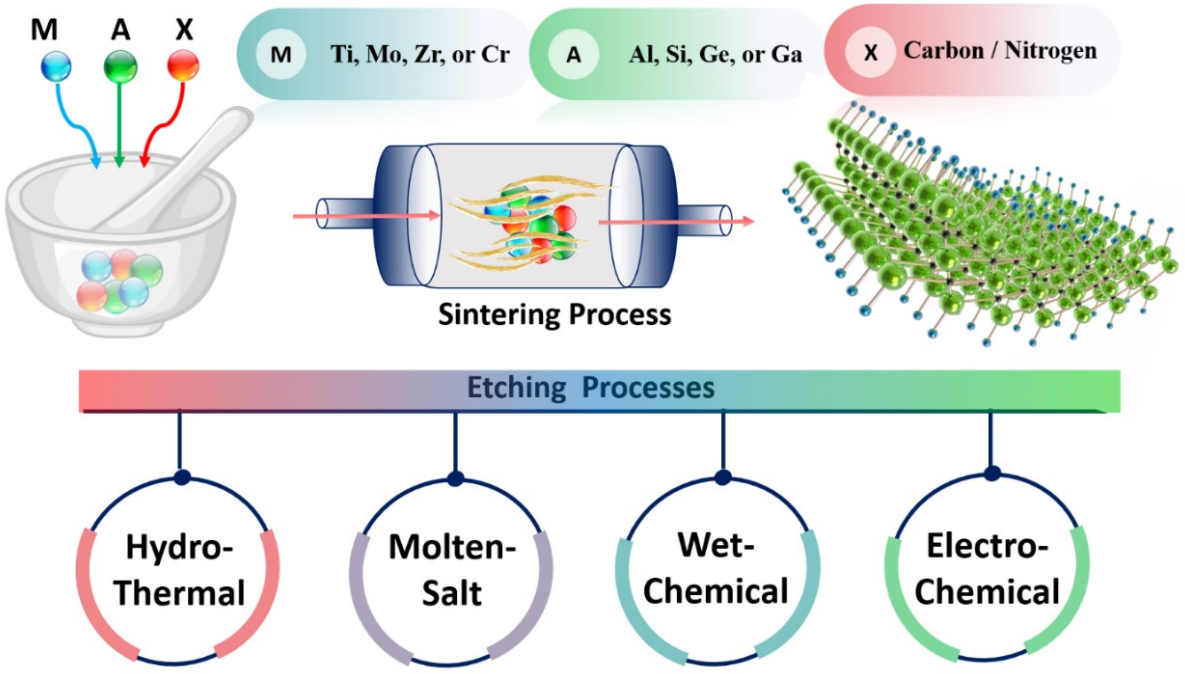

Figure 3. Chemical structure, as well as common etching processes of the MXene nanosheets.

The molten $ZnCl_2$ is strongly Lewis acidic, allowing Zn atoms to replace A-site elements in the MAX precursor, like Al in Ti_3AlC_2. When excess $ZnCl_2$ salt is used, the Zn atoms can be detached, resulting in Cl-terminated MXenes. This strategy has been extended to various A-

site elements, including Zn, Si, Al, and Ga, from different MAX precursors, like Ti_2AlC and Ti_3AlCN. It is attained through selective A etching carried out by a reaction between the A elements and the Lewis acid molten salts. This approach could further lead to expanding the MAX family and enabling the synthesis of MXenes without any surface functional groups. For example, Talapin et al. deployed an approach to hinder surface functional groups by applying the molten salt strategy [53]. They successfully synthesized MXenes with various terminations, including -O, -NH, -Cl, -S, -Br, -Se, and -Te, as well as pristine MXenes. These MXenes exhibit unique properties, such as Nb_2C MXenes showing surface group-dependent superconductivity [54].

MXenes exhibit favorable characteristics, including high electrical conductivity, exceptional stability in various electrolytes, and good mechanical strength, making them a promising option for various electrochemical applications, particularly in energy storage systems like batteries and supercapacitors [55]. The high electrical conductivity and large surface area of MXenes make them ideal electrode substances for devices capable of storing energy. Researchers have revealed the outstanding specific capacitance, cycling durability, and rate capability of MXenes, making them potential for efficient supercapacitors [56]. Another interesting application of MXenes is in electrocatalysis. MXenes have shown excellent catalytic activity for various electrochemical reactions, including oxygen reduction reaction (ORR), hydrogen evolution reaction (HER), and water oxidation reaction (WOR) [57]. It is widely declared that MXenes can meaningfully augment the catalytic activity and steadiness of electrocatalysts due to their unique surface chemistry and electronic structure [58]. MXenes have also shown promise as electrochemical sensors for detecting various heavy metal ions, neurotransmitters, and glucose analytes. It is observed that these structures possess excellent electrocatalytic activity for various analytes, making them promising candidates for developing high-performance

electrochemical sensors [59]. Besides, MXenes have also been employed in other electrochemical devices, such as electrochemical capacitive deionization (CDI) [60], electrochemical water splitting [61], and electrochemical biosensors [59]. Overall, MXenes have emerged as promising applicants for numerous electrochemical applications, such as energy storage, electrocatalysis, electrochemical sensing, and water treatment, which could play a significant role in progressing the electrochemistry field with further growth and progress.

3. MXene-loaded nanofibrous actuators

Electrospun actuators are a type of electrochemical active device commonly made through an electrospinning procedure. These electrochemical nanofibrous structures experience contraction/expansion in response to the electric field, creating a bending or twisting motion. Therefore, a variety of mechanical movements, including gripping, crawling, or twisting, could be provided by converting the environmental signals. The high specific surface area of the electrospun fibers allows a larger surface area of the electrochemical actuators to be exposed to the electrical field, resulting in a stronger and more efficient response. Additionally, the electrospun actuators could be shaped in different forms and sizes, which is a valuable factor in representing worthwhile applications in a diverse range of fields, such as robotics, biomedical engineering, and microelectrochemical systems. Compared with the casted actuators, the electrospun shape memory polymers provide a higher surface area, greater flexibility, improved mechanical characteristics, superior sensitivity, and enhanced functionality. Additionally, outstanding electrical conductivity could be endowed through the introduction of two-dimensional nanomaterials into electrochemical polymeric composites. MXene is assumed as an emerging material in actuator devices, which could act as humidity-, photothermal-, electronic-, and electrochemical-responsive materials. As an example, Wu et

al. [28] first fabricated the electrospun polyether-based shape memory polyurethane structure, followed by hybridizing and dispersion of $Ti_3C_2T_x$ MXene/cellulose nanocrystals onto the nanofibers. Accordingly, a highly porous fibrillar structure with proper flexibility and stretchability was formed. Also, the MXene/cellulose hybridized structure was well and uniformly dispersed onto the fabricated nanofibers. The prepared structure exhibited superior mechanical behavior through providing more stretchability, as well as elongation to break. In addition, an increase in the cellulose concentration caused an enhancement of Young's modulus up to 2.8 MPa, due to its high modulus and stress-transferring ability via the hydrogen bonding network. The interaction of the polymeric substrate and the deposited nanostructure was corroborated through the shifting of the glass transition temperature. The NIR stimulation was conducted, showing 80% extension in the sample within 10 s for elating an object with a weight of 265 times (see **Figure 4a**).

In another effort, polydopamine was modified with $Ti_3C_2T_x$ MXene/bacterial cellulose nanofibers to obtain a humidity-responsive actuator, resulting from its appropriate hydrophilicity, as well as conductivity of the MXene nanosheets. **Figure 4b** depicts the schematic illustration of the designed structure in response to moisture. As shown, strong hydrogen bonding could be created between water vapor and MXene, cellulose, and polydopamine. The formed bonding is able to weaken the cellulose-polydopamine/MXene interaction, leading to an increase in the space between the cellulose nanofibers and the polydopamine flakes. Therefore, the polydopamine hydrophilic layer is first influenced by the water molecules, causing the nanoflake's expansion. The remaining water molecules are also captured by the bacterial cellulose, causing the creation of a framework with gradient expansion in the thickness direction, and so forcing it to bend. **Figure 4c** shows the bending of the samples in the humidity of 40%. Excellent stability in the bending/unbending cycling is

also figured out in **Figure 4d**. Great electrical conductivity of the synthesized actuator caused high sensitivity even in the presence of a finger, which is depicted in **Figure 4e** [62]. In another approach, Pang et al. [63] deployed an electrochemical actuator using the symmetric $Ti_3C_2T_x$ MXene electrode separated by PVA−H_2SO_4 gel electrolyte. Since robotic actuators are forced to work in air, a prototype of the solid-state MXene-based actuators is proposed in this study (see **Figure 4f**). The galvanostatic charge/discharge cycles at 500 mAg^{-1} were also conducted for 10,000 cycles, showing a self-improving performance up to 1000 cycles mighty because of enhanced proton permeation between the MXene layers (see **Figure 4g**).

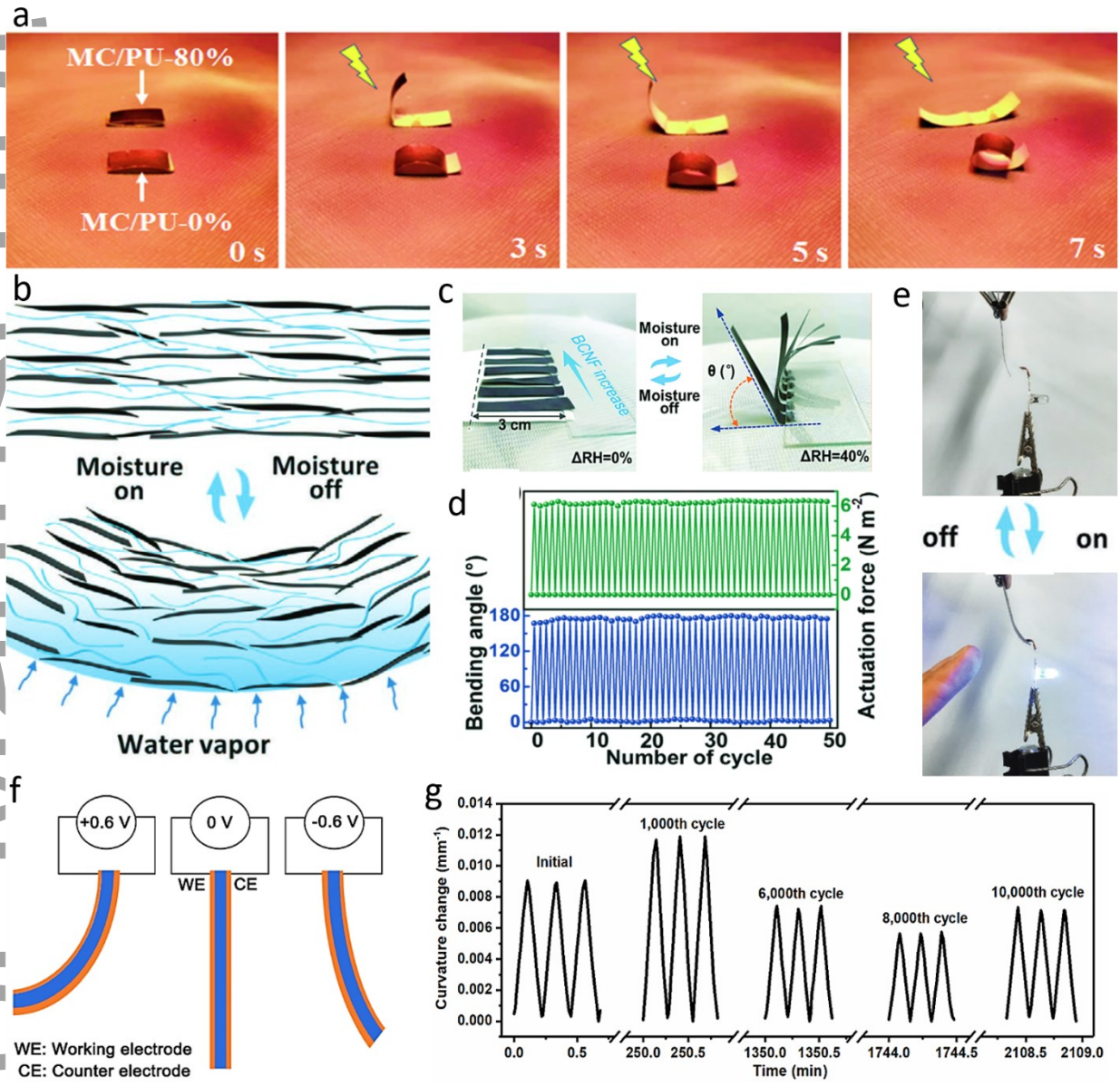

Figure 4. Characteristics of the $Ti_3C_2T_x$/cellulose crystal deposited on an electrospun mat; (a) NIR-activated actuator in extended and bent states. Reproduced from reference [28] with permission from Elsevier. Features of the MXene/Cellulose/Polydopamine film; (b) actuation mechanism in response to moisture, (c) bending of the prepared composite in the presence of 45% humidity, (d) cycling performance, and (e)sensitivity of the sample in the presence of finger with a distance. Reproduced from reference [62] with permission from Wiley. Properties of the MXene-based electrochemical actuator; (f) bending prototype and (g) the galvanostatic charge/discharge at 500 mAg^{-1}. Reproduced from reference [63] with permission from the American Chemical Society.

Although promising roles of the electrospun fibers in fabricating versatile actuators, as well as MXene in the synthesis of sensitive actuators in various conditions have been declared in various studies, developing of the electrospun networks decorated with MXene nanosheets has rarely been studied, which could be considered in future evaluations. Moreover, it is important to examine and address some potential disadvantages and limitations that may impact the application of actuators due to the presence of MXene nanosheets. While MXene materials exhibit high electrical and thermal conductivity, certain compositions may not possess the same level of mechanical strength and structural robustness required for reliable actuation over extended periods. Also, some compositions may have limitations in their elastic modulus and flexural stiffness, potentially impacting their ability to withstand repeated actuation and deformation cycles without experiencing wear or fatigue. Additionally, MXene-based actuators might be susceptible to environmental factors, such as water sensitivity, potentially impacting actuator performance and long-term stability in certain operating conditions. Careful consideration of potential safety and health implications associated with MXene-based actuator structures is essential due to the presence of metallic atoms, particularly in prolonged or high-exposure scenarios.

4. The electrospun battery components integrated with MXene

The urgent requirement for sustainable energy storage tools has made lithium-ion batteries (LIBs) a prominent part of everyday life [64]. LIBs offer several advantages over other energy-storage devices, as highlighted in various attempts, including possessing the lowest reduction potential of any element, which makes them more efficient [65], the choice of power source for portable electronic devices [66], having a higher energy density and lower maintenance compared to other rechargeable battery technologies [67, 68], exhibiting fast charge-discharge

characteristics with proper structural stability, as well as high electrical and Li^+ ion conductivity [69-71]. Recent advancements in lithium-ion battery research stem from the development of new chemistries beyond LIBs, which have led to better performance of the anode, cathode, and electrolyte materials [72]. Additionally, there have been recent discoveries in LIB technology that are expected to push the energy limit in the coming years [73, 74].

MXenes are deemed a family of 2D structures exhibiting promise in several energy storage applications, including LIBs, with the potential to improve the devices' performance [75]. Specifically, Ti_3C_2 MXene has been studied for its electronic characteristics and the ability to store Li ions. According to the literature, recent research has been attentive on developing 2D MXene-based hybrid substances for next-generation energy storage and LIBs [76]. Likewise, MXenes have exceptional possessions, such as a layered structure that makes them suitable for anode materials by offering a high specific capacity of 320 mAh g^{-1} at 100 mAg^{-1} current after 760 cycles [77]. Although graphitic carbon is currently assumed to be the most valuable material for the LIBs' anode, MXenes have the potential to substitute due to their astonishing electrochemical properties [78].

Despite the brilliant properties and advantages of this class of materials, there are still some challenges in using MXenes as anodes in LIBs. One of the main hurdles is linked to their lower specific capacity compared to other anode materials [79]. Another setback is the tendency of MXenes to agglomerate, which can lead to a reduction in their electrochemical performance [80]. The intercalation of certain electrolyte ions into MXene layers may not always be as efficient, potentially leading to uneven ion distribution and hindered performance. Also, some MXene materials may have limited stability in aqueous environments, resulting in potential degradation and reduced performance, particularly in aqueous electrolyte-based systems. Over prolonged cycling, some MXene compositions are susceptible to exhibit deterioration in

performance and structural integrity, hindering long-term cycling stability. Additionally, the synthesis of MXenes could be complex and expensive, limiting their large-scale production [80]. Nevertheless, the research is ongoing to overcome these limitations through revealing some strategies, including improving synthesis procedures [7, 81], combining MXenes with other constituents (e.g., carbon or silicon nanoparticles) [82, 83], exploring the utilization of MXenes in post-LIBs [84], and developing new MXene-based materials (e.g., double transition metal MXenes) [85, 86]. The stability of MXenes is also focused on upgrading the storage level and cycle life of energy storage devices [87]. In terms of performance and sustainability, numerous studies have demonstrated that MXenes can exhibit pseudo-capacitance and are capable of storing Li-ions reversibly, such as yielding a reversible discharge capacity of 355 mAh g^{-1} at a current rate of 1000 mAg^{-1} over 1300 cycles for $MoS_2@Ti_3C_2$ MXene composite [79]. Also, TiO2-encrusted MXene is a high-performance anode for LIBs [88].

MXene nanofibers have been extensively examined for their potential use in LIBs. They have low theoretical Li^+ diffusion barriers, proper energy densities, and excellent conductivity, making them promising electrode materials for lithium-ion storage [89, 90]. MXene-based composites and hybrids have also been discovered for their multifunctional applications in energy storage power tools. MXenes with wider interlayer spacing, low diffusion barriers, and high electrical conductivity can provide admirable rate performance and cycling durability in LIBs [89, 90]. Therefore, it is necessary to explore the potential of MXene nanofibers and their composites with other functional materials in LIBs and overview their performance and prospects. MXene nanofibers have several advantages when used in LIBs and can also improve the performance of LIBs in several ways. They have shown wider interlayer spacing, low diffusion barriers, superior lithium capacity, proper conductivity, and a low operating voltage, enabling them to reveal admirable cycling durability and rate performance [90].

MXenes are also tunable in terms of their elements and surface groups, making them promising electrode constituents for Li^+ ion storage. Additionally, MXene-based composites and hybrids have shown exceptional theoretical storage capacity, desired mechanical and electrical properties, and high specific capacity after cycling. These composites could be prepared using various materials and through different methods, mainly with Si and/or carbon nanofibers (CNFs) via electrospinning [91-93]. The employed MXene in the mentioned composite structures may vary depending on the targeted properties and application. However, some commonly used MXenes in the LIB structures are $Ti_3C_2T_x$ [94], Ti_2CT_x [95], and $Ti_3C_2(OH)_{0.8}F_{1.2}$ [96].

Guo et al. [97] designed a Fe_3O_4@MXene/CNFs as a versatile anode in LIBs, reporting that the electrospinning process could tackle the problem of Ti_3C_2 flakes self-restacking, as well as Fe_3O_4 aggregation, giving a higher specific surface area, along with more active sites on the anode structure. The SEM and TEM images of the prepared structures are revealed in **Figures 5a-d**. The cycling performance of the specimens is also provided at 2 Ag^{-1} in **Figure 5e**, representing the discharge capacity increment after the 5th cycle due to the electrode lithium-induced reactivation. Therefore, the produced 3D conductive network could boost the cycling stability of Fe_3O_4, while the MXene-free structure exhibited a lower capacity of 612 mAh g^{-1} because of the structural deconstruction during the cycling process. According to the Nyquist plot (**Figure 5f**), the charge transfer impedance could also be declined using the MXene in the structure.

In further similar research related to this, MnO_x-MXene/CNF anode could form a 3D network with outstanding stability and conductivity, leading to outstanding electrochemical characteristics, such as 1268 and 1137 mAh g^{-1} at 2 and 5 Ag^{-1}, conforming to a specific capacity of 2.536 and 2.274 mAh.cm^{-2} at 4 and 10 mA.cm^{-2}, respectively [98]. The charge storage mechanism of MXenes in LIBs has been evaluated by exploring the mechanism of

electronic features and the ability of Li storage in Ti_3C_2 and $Ti_3C_2X_2$ (X=F, OH) monolayers [99]. Therefore, the obtained data suggested a new design principle for the MXene anode through reducing the lateral size to achieve a dilated interlayer spacing and reduced diffusion path [100]. The characteristics of $Si/Ti_3C_2T_x$ MXene nanofibrous composites in LIBs have also been studied, offering benefits like the buffer layer acting on flexible MXene nanosheets resulting in advanced capacity retention, the strong anchoring of SiNPs to the MXene nanosheets, and more effective transportation channels for Li^+ ions [101, 102].

Similar to the composites with carbon, hollow Ti_3C_2 MXene/carbon nanofibers could address the limitations of 2D MXene electrodes in several ways. Firstly, they have an increased specific surface area, providing higher active sites for storing Li^+ ions. Secondly, they have tailored surface terminations, which can progress the conductivity of the composites. Finally, the carbon framework of the nanofibers is auspicious to the composites' conductivity and can overcome the low surface-to-volume ratio and disturbance of Li^+ ion diffusion [89]. In recent research, a novel multi-protuberant nanofiber structure was formed by making the composition of 2D Ti_3C_2 nanosheets, and 0D $ZnCo_2O_4$ nanoparticles within 1D carbon nanofibers. Schematic illustration of the employed electrospinning set-up, as well as the SEM images before and after the carbonization procedure, are presented in **Figures 5g-i**, respectively. **Figure 5j** also depicts the TEM image of the designed structure after the carbonization procedure. The cycling performance of the $ZnCo_2O_4$@carbon nanofibers integrated with various MXene amounts of 0, 25, 75, and 100 mg is provided in **Figure 5k**, representing a high initial capacity in the low MXene content, in contrast, the cycling stability could be boosted in the high MXene contents. In conclusion, the synergetic effects of the right MXene proportion, $ZnCo_2O_4$, and carbon nanofibers could lead to approaching proper electrochemical performance. A small polarization effect was also declared for the optimized

Ti_3C_2@$ZnCo_2O_4$@carbon nanofibers based on the CV curves at sweep rates from 0.1 to 10 mV s^{-1} (**Figure 5l**). Furthermore, it was shown that a rise in the MXene content up to 100 mg could affect the conductivity positively, resulting from the rapid lithiation/delithiation (**Figure 5m**) [103].

Table 1 summarizes various advancements carried out toward the integration of batteries' performances using networks filled with MXene nanosheets.

Table 1. Progress in the performance of battery structures using MXene nanosheets.

Designed structure	Outcome	Performance	Ref.
Electrospun PAN/PU/$Ti_3C_2T_x$ framework as a battery separator in Zn batteries	-The addition of MXene caused an increment in the porosity value, possibly due to the formation of finer fibers. -The presence of hydroxyl groups in the MXene terminal groups led to the enhancement of wettability. -The ionic conductivity was also improved through the MXene addition, resulting from an increase in carrier channels.	2214% electrolyte uptake and 3.35 mS cm^{-1} ionic conductivity	[104]
Core-shell MXene/Si@C nanofibrous structure as anode material in Li batteries.	-Conductive nanofibers were formed by enhancing the contacts between Si particles via the presence of MXene nanosheets. -Loading MXene and carbon shell in the structure caused double	Initial Coulombic efficiency of 78.4% and high capacity of 1083 mAh g^{-1} at 0.1 Ag^{-1}	[105]

	accommodation for Si volume change, which could maintain the structural durability during the cycling. -Frequent functional groups in the MXene and carbon shell led to the improvement of the battery capacity.		
$Ti_3C_2T_x$ MXene/carbon heterostructure for Li-CO_2 batteries	-The CO_2 adsorption was enhanced with the high catalytic performance of MXene nanosheets, as well as the desirable stability of carbonous materials.	Specific capacity of 11,458 mAh g^{-1} at 200 mAg^{-1}	[106]
Carbon nanofibers integrated with manganese ion-modified MXene nanosheets	-The presence of MnO_x inside the nanofibers and on their surfaces caused enhancing the structural stability. -Electrospinning procedure prevented MXene restacking, leading to the creation of an anode structure with a larger surface area.	Reversible capacity of 1098 mAh g^{-1} at 2 Ag^{-1} after 2000 cycles	[107]
Layer-by-layer coating of MXene nanosheets and multi-walled CNT on electrospun PCL nanofibers as battery electrodes	-Capacitance retention of the structure was enhanced likely due to the provided highly porous and interconnected structure without MXene nanoflakes restacking.	Around 100% capacity retention and Coulombic efficiency after 10000 cycles	[108]

Hollow Ti_3C_2 MXene/carbon nanofibrous anode for LIB structures	-The formation of a hollow structural network provided superior energy density, resulting from an enhancement in the surface-to-volume ratio, a reduction in the nanosheets' restacking, and an increase in the functional groups.	306.5 mAh g^{-1} at 40 mAg^{-1}	[89]
Ti_2SnC/CNFs hybridized anode structure	-The presence of MXene in the structure led to a significant reduction in the SEI irreversible formulation, as well as enhancing the Coulombic efficiency. -Participation of more Ti_2SnC in the electrochemical reactions caused the formation of a more pronounced cathodic peak.	367.5 mAh g^{-1} at 1 Ag^{-1} after 500 cycles	[109]

Based on the literature, cost-effective and efficient electrode materials are designed and prepared. Accordingly, the synergetic effects of the MXene nanostructures and the electrospun nanofibrous networks could be much more efficient than conventional conductive polymer nanocomposites in the LIBs.

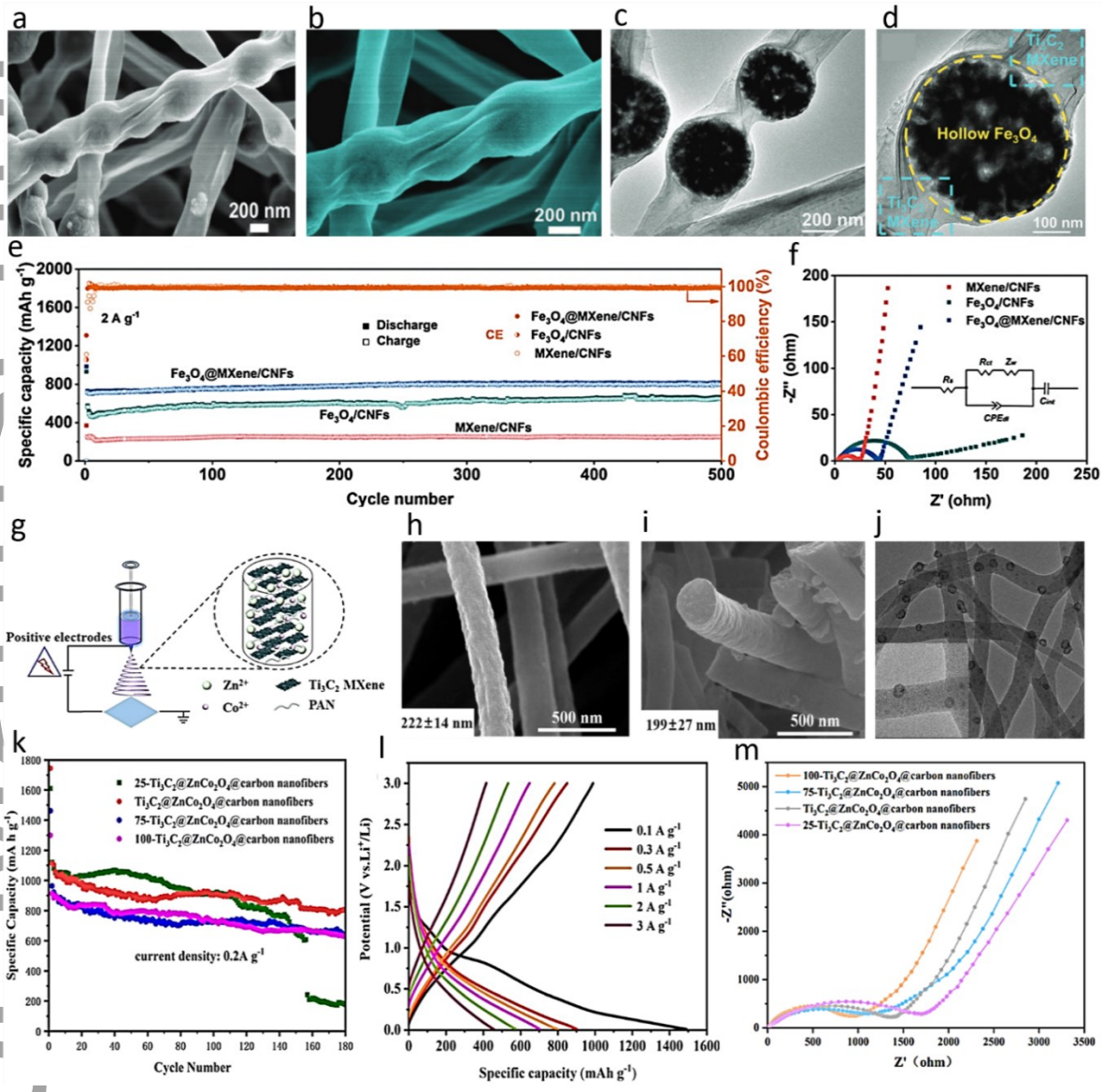

Figure 5. Properties of the Fe_3O_4@MXene/CNFs anode structure; (a&b) SEM images, (c&d) TEM illustrations, (e) cycling performance, and (f) Nyquist plot. Reproduced from reference [97] with permission from the Royal Society of Chemistry. Characteristics of the Ti_3C_2@$ZnCo_2O_4$@carbon nanofibers; (g) the employed electrospinning apparatus, (h) SEM image before the carbonization, (i&j) SEM and TEM images after the carbonization step, (k) cycling performance at 0.2 Ag^{-1}, (l) CV curves at 0.1 to 10 mV s^{-1} sweep rates, and (m) the Nyquist plots. Reproduced from reference [103] with permission from the American Chemical Society.

5. Employing MXene in the structure of electrospun Fuel cells

The direct conversion of chemical to electrical energy makes fuel cells (FCs) a sustainable harvesting technology. Energy harvesting is a key building block toward deploying autonomous self-powered microelectronic devices [110]. It is found that the hydrophilic surface of MXene makes feasible the process of composite formation with polymers, carbon components, or other metal oxides. The tunable surface properties of MXene open new pathways to evaluating the material for various possible applications. Although MXene comes across to a large extent of applications, the literature in the form of a review on a specific application of fuel cells is rare [111-113].

In the last two decades, microbial fuel cells (MFCs) have gained a lot of scientific and technological attention in the renewable energy resource category. Implementation of MXene as an anode material has been carried out to resolve obstacles associated with poor electron transfer and bacterial adhesion of MFCs. According to Liu et al. [114], the multilayer framework, excellent conductivity, and high surface area of Ti_3C_2 offer sufficient nutrition for microbial growth, which are essential for mass transfer and facilitate active sites for catalytic redox reactions. SEM images and contact angles of the pristine carbon clot (CC) and the Ti_3C_2/CC are shown in **Figures 6a-d**. Covering the surface with mxene enhanced the hydrophilicity and lowered the contact angle from 140 to 114º. Compared with CC, the sandwiched CC with 1.15 mg cm^{-3} of Ti_3C_2 caused the increment of power density from 2.05 $W.m^2$ to 3.74 $W.m^2$ and approached higher capacitive current due to the ultrahigh active surface area and more active sites that facilitate the necessary redox reaction (see **Figures 6e&f**). Excellent electrical conductivity of MXene structure and surface tunability can show feasible properties in low-temperature fuel cells like PEMFCs (> 100ºC). Fei et al. [115] found that the proton conductivity, as well as power density, could be enhanced through the addition of 3% $Ti_3C_2T_x$ in polybenzimidazole at 90ºC and 80% humidity (see **Figures 6 g&h**). However, the results

showed that excessing the Mxene content higher than 3% could result in lower proton conductivity and power density due to the agglomeration of MXene sheets.

Oxygen reduction reaction (ORR) is deemed a critical factor in approaching a high-performance fuel cell. Therefore, Pt-based electrocatalysts are commonly employed, but they are not durable and cost-effective. To address these obstacles, non-Pt-based catalysts are applied because of their high efficiency and stability. Besides various studied non-Pt electrocatalysts, such as N-doped graphene and carbon-based catalysts, the MXene family has shown superior redox activity, as well as appropriate hydrophilic properties mighty due to their high surface area, charge carriage ability, and long-lasting durability [116, 117]. Wang et al. [25] embedded Mo_2C into the PVP nanofibers in the electrospinning condition of 20 kV voltage, 10 $\mu l.min^{-1}$ feeding rate, 15 cm distance, and a needle diameter of 1.6 mm. Then, the produced fibers were calcined at 450ºC for 1h and 850ºC for 3h under H_2/Ar atmosphere to attain nanoporous carbon fibers enriched with Mo_2C. **Figures 6i-l** show the synthesized electrospun nanofiber in this attempt. Accordingly, the provided electrocatalyst exhibited the ORR activity with an onset potential of ~0.9 V, a Tafel slope of 60.2 mV dec^{-1}, and a durable activity over 10h (see **Figure 6m**). This could be linked with the development of new active sites through the addition of Mo_2C to the structure.

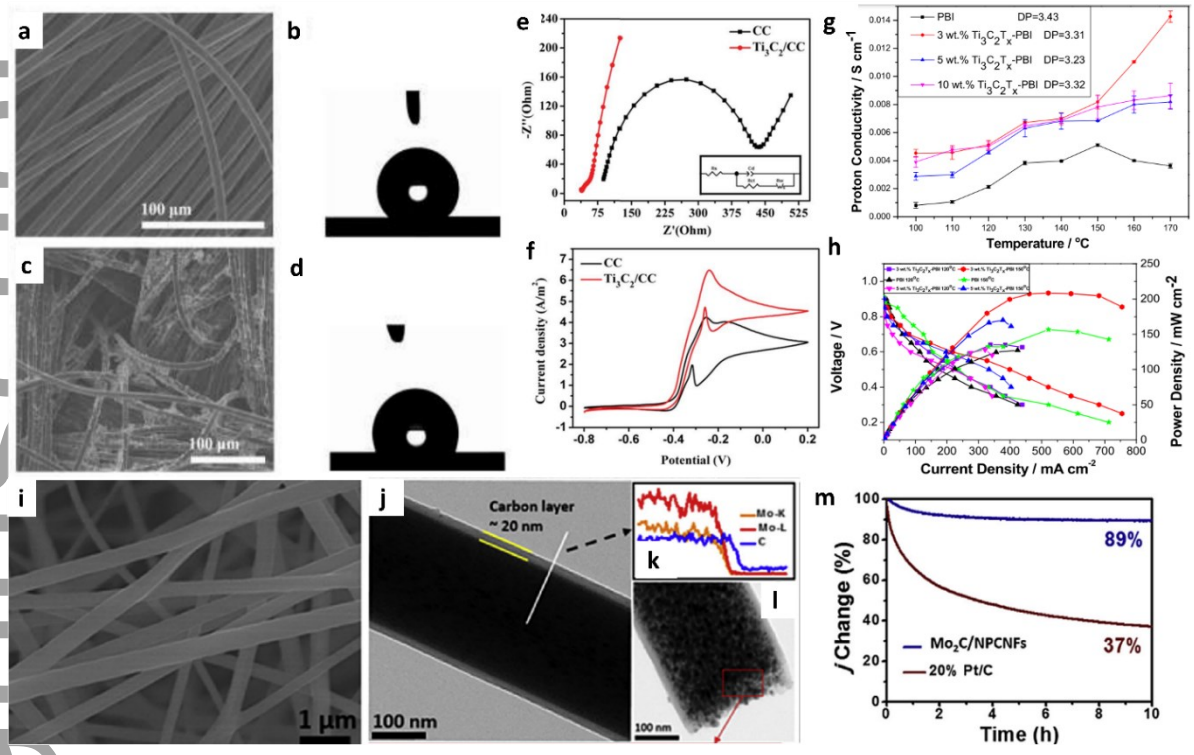

Figure 6. The performance of Ti_3C_2/CC structure; (a) SEM image of the CC nanofibers, (b) contact angle of the pristine CC clot, (c) SEM image of the Ti_3C_2/CC structure, (d) contact angle of the Ti_3C_2/CC, and their (e) Nyquist plot and (f) current density. Reproduced from reference [118] with permission from the Royal Society of Chemistry, characteristics of $Ti_3C_2T_x$/polybenzimidazole; (g) proton conductivity and (f) power density. Reproduced from reference [115] with permission from IOPScience, and PVP nanofibers incorporating Mo_2C; (i-l) illustrations of the fabricated fibers and (m) change ratio during time. Reproduced from reference [25] with permission from Elsevier.

There is vast research in fuel cells, demanding composite constituents with proper mechanical strength, good in-plane and through-plane conductivity, robustness, and tunable porosity to defeat the challenges of their metals in corrosive environments. The free-standing properties of nanofiber and the highly valued property MXene, along with their combination, have lots of scope for study in the development of efficient materials for the advancement of fuel cell quality as alternate energy in the near future. These advanced nanofiber-MXene composites

not only promise to enhance fuel cell performance but also open up new possibilities for designing lightweight and compact fuel cell systems. Delving into the world of MXene in fuel cell structures, a variety of advantages has been encountered, however as with any material, there are some drawbacks to consider as well. Some variants of MXene family may exhibit limited stability in certain chemical environments, such as strong acids or bases. This can pose challenges in the context of fuel cells, where the electrolyte and operating conditions can be quite aggressive. Chemical instability could lead to performance degradation and impact the overall durability of the fuel cell. Also, MXene materials may not provide sufficient barrier properties against the permeation of air or water vapor. In fuel cells, particularly those that operate at elevated temperatures and pressures, effective gas and liquid barriers are crucial to prevent contamination and maintain high efficiency. This permeability issue could limit the utility of certain MXene materials in fuel cell structures. While some MXene architectures possess intrinsic catalytic activity, it is significant to note that not all configurations of MXene may exhibit desirable catalytic properties for fuel cell reactions. Tailoring MXene for optimal catalytic performance in the harsh electrochemical environment of fuel cells remains an active area of research and development. Over extended usage, some MXene materials may be prone to degradation, potentially impacting the long-term stability and performance of fuel cells. Understanding and mitigating this degradation is essential to ensure the durability and reliability of fuel cell systems incorporating MXene.

6. Electrospun electrochemical biosensors incorporating MXene

2D layered MXene materials have been exploited in biosensor applications due to outstanding features such as amazing conductivity (10,000 S cm^{-1}), thermal stability, ion intercalation behavior, speedy mass diffusion through the electrodes, hydrophilic surface, and so forth. The

combination of MXene's outstanding characteristics with the unique features of the electrospun arrays has led to approaching electrochemical sensors with ideal reproducibility, repeatability, reusability, and stability [23]. Ranjith et al. [119] fabricated coaxial fibers with ultra-thin MXenes for rutin (3′, 4′, 5, 7-tetrahydroxy-flavone-3-d-rutinoside; RT) detection. First, 13 wt. % of PAN: PMMA (0.6:0.4) was dissolved in DMF, followed by the addition of 0.2 g WCl_3 and 0.2 g $FeCl_3$. Then, the electrospinning process was conducted at 17.5 kV voltage, 1 ml h^{-1} flow rate, and 15 cm electrospinning distance (see **Figure 7a**). Afterward, the collected nanofibers were dried overnight and calcinated at 550°C for 3h to gather $FeWO_4$ composite. Simultaneously, $Ti_3C_2T_x$ was created via an acid-based selective approach.

For the synthesis of MXene-$FeWO_4$ core-shell nanoarrays, MXene was added dropwise into the $FeWO_4$/ethanol solution and heated for 10h at 140°C. The hybrid electrode design is schematically illustrated in **Figure 7b**. In order to prepare the electrochemical sensor, 3 µL of MXene-$FeWO_4$ consistent suspension in ethanol was drop-casted on a clean GCE, dried in an oven at 40°C for 15 minutes, and rinsed with water to eliminate unbounded nanocomposite. Accordingly, fibers with an approximate average diameter of 300 nm with appropriate pore structure and favorable interface features were formed after the calcination procedure (see **Figure 7c**). As shown in **Figure 7d**, a 0.42 nM detection limit, 4-147 nM linear range detection, and 0.3799 µA $nM^{-1}cm^{-2}$ sensitivity of were gained. Regarding reproducibility, six different electrodes were analyzed in the same condition (40 nM RT in 0.05 M PBS pH=7.0), displaying 3.18% RSD for the MXene-$FeWO_4$ GCE oxidation peak. The repeatability of the electrode was also figured out to be 3.26% RSD in the same condition. Moreover, the results highlighted the 2.42% RSD of detection reusability. Based on **Figure 7e**, the impedance was slightly decreased to 34 Ω through integrating the GCE with the MXene/$FeWO_4$ because of the high surface area and proper electrical conductivity of the MXene/$FeWO_4$. **Figure 7f** also depicts the CV curves,

implying the enhancement of oxidation and reduction with rising scan rates. Also, a linear shift to the negative potential direction was observed, declaring superior electron transfer kinetics, as well as better adsorption capacity. Furthermore, 81% of the stability could be retained after 30 days, completely relating to the presence of abundant active sites on the MXene-$FeWO_4$ GCE that provide high electro-catalytic activity and outstanding electrochemical sensing for RT detection.

In another work, Al-Dhahebi et al. [120] reported an aptasensor electrode made by MXene/polyvinylidene fluoride ($Ti_3C_2T_x$/PVDF) nanofibers for ochratoxin A (OTA) detection. OTA is a secondary fungal metabolite mycotoxin classified as a group 2B carcinogen in humans because of immunotoxicity, teratogenicity, and neurotoxicity by the International Agency for Research on Cancer. So, a reliable detection method with high selectivity and sensitivity is prominent to customize OTA. In the first step, $Ti_3C_2T_x$ was synthesized by the MILD method, then $Ti_3C_2T_x$ flakes were dispersed in DMF for 1.5h and centrifuged at 8500 for 25 min. Next, different $Ti_3C_2T_x$ concentrations (0, 5, 9, and 13 wt. %) were introduced into 20% (w/w) PVDF solution in DMF/acetone (3:2) v/v and stirred for 24h at room temperature. All samples were electrospun using 18 kV voltage, 15 cm electrospinning distance, 2 $ml.h^{-1}$ flow rate, 1000 rpm rotary collector, and 30% relative humidity for 6h.

Screen printed-carbon electrodes (SPCE) were covered with 8 $mg.ml^{-1}$ $Ti_3C_2T_x$/PVDF nanofibers suspensions in DMF. The previous suspensions were prepared under bath sonication for 15 min at RT, then 10 µL of fibrous suspension was drop-casted onto SPCE as a working electrode and left to dry for 2h at RT. Notably, (3-Aminopropyl) triethoxysilane (APTES) and glutaraldehyde were used to immobilize OTA-aptamer. According to the results, the diameters of the fabricated bead-free fibers were enlarged from 71-80 to 219-230 nm by increasing the $Ti_3C_2T_x$ from 0 to 13 wt. %. This could be accredited to the retaking of $Ti_3C_2T_x$ fluorine groups

with that of PVDF and also, the slow rate of solvent evaporation because of the interplay between the hydrophilic surface of MXene and humidity [121]. The analytical performance of produced aptasensors was examined by the EIS method with distinct concentrations of OTA in the range of 1 fg ml^{-1} to 1 ng ml^{-1} in 20 µL PBS, resulting in the R_{ct} increment with rising OTA concentration, mighty because of OTA non-electroactive molecules that diminish electron transfer within the electrode interface. Moreover, the optimized aptasensor depicted high selectivity and sensitivity with an LOD of 2.15 fg ml^{-1}, LOQ of 6.52 fg ml^{-1}, and wide linear range detection of 1 fg ml^{-1} to 1 ng.ml^{-1} which is applicable to detecting OTA in the food industry.

Sharifuzzaman et al. [122] developed an electrochemical-electrophysiological multimodal biosensing patch comprising MXene/fluoropolymer nanofibrous structures integrated with hierarchical porous TiO_2 nanocrystals over 3D fibrous carbon nanohybrid electrodes. It is worth noting that electronic textiles have been remarked for medical treatment and healthcare due to comfortable and accurate monitoring of chemical-physiological aspects. The multi applications of the designed composite are illustrated in **Figure 7g**. In this research, 17 wt. % poly(vinylidene fluoride) (PDFE) and 15 wt. % MXene were used to fabricate bead-free nanofibers. Based on the results, H-bond interaction could be formed between MXene functional sites (-OH, -O, and –F) and the orientation groups of the β-phase CF_2-CH_2 chain in PDFE. The fabricated mats were carbonized by direct CO_2 laser with 10% speed and 6.5% power. The high heat in laser irradiation caused the placing of TiO_2 nanoparticles on the 3D carbon nanofibers (CNFs), which is shown in **Figure 7h**. The TiO_2 forming could be completely related to Ti thermal activity of $Ti_3C_2T_x$ in the presence of T_x during laser-carbonaceous. The produced sensor was utilized for electrochemical-physiological monitoring, including pH, glucose, and ECG in a volunteer's sweat. Regarding glucose detecting, Pt

nanoparticles (25 segments) were employed as a catalyst, while PANi coatings (50 segments) were electropolymerized over TiO_2@LCNFs for pH sensing. Based upon the results, the accumulation of MXene nanosheets was discovered in the bead-free fabricated fibers with increasing the MXene concentration up to 20 wt. %. After 5 days of monitoring the redox peak separation, the oxidation peak only shifted 20 mV, displaying its appropriate stability with strong adhesion. The applied laser power had a prominent impact on the electroactive area and electron transfer kinetics. Moreover, the current density was increased with anatase TiO_2 and large pore sizes due to enhanced electroactive area. The peak redox potential separation (ΔEp) for various LP were estimated as TiO_2@LCNFs (6.5%) < TiO_2@LCNFs (7%) < TiO_2@LCNFs (6%) < TiO_2@LCNFs (5.5%) < PDFE (6.5%), corroborating the best electron transfer kinetic in the TiO_2@LCNFs structure (see **Figure 7i**). Furthermore, the designed patch was enabled to monitor sweat glucose with pH adjustment, presenting the 77.12 μA $mM^{-1}cm^{-2}$ sensitivity within 0.01-2×10^{-3} M physiological concentrations (see **Figures 7j&k**).

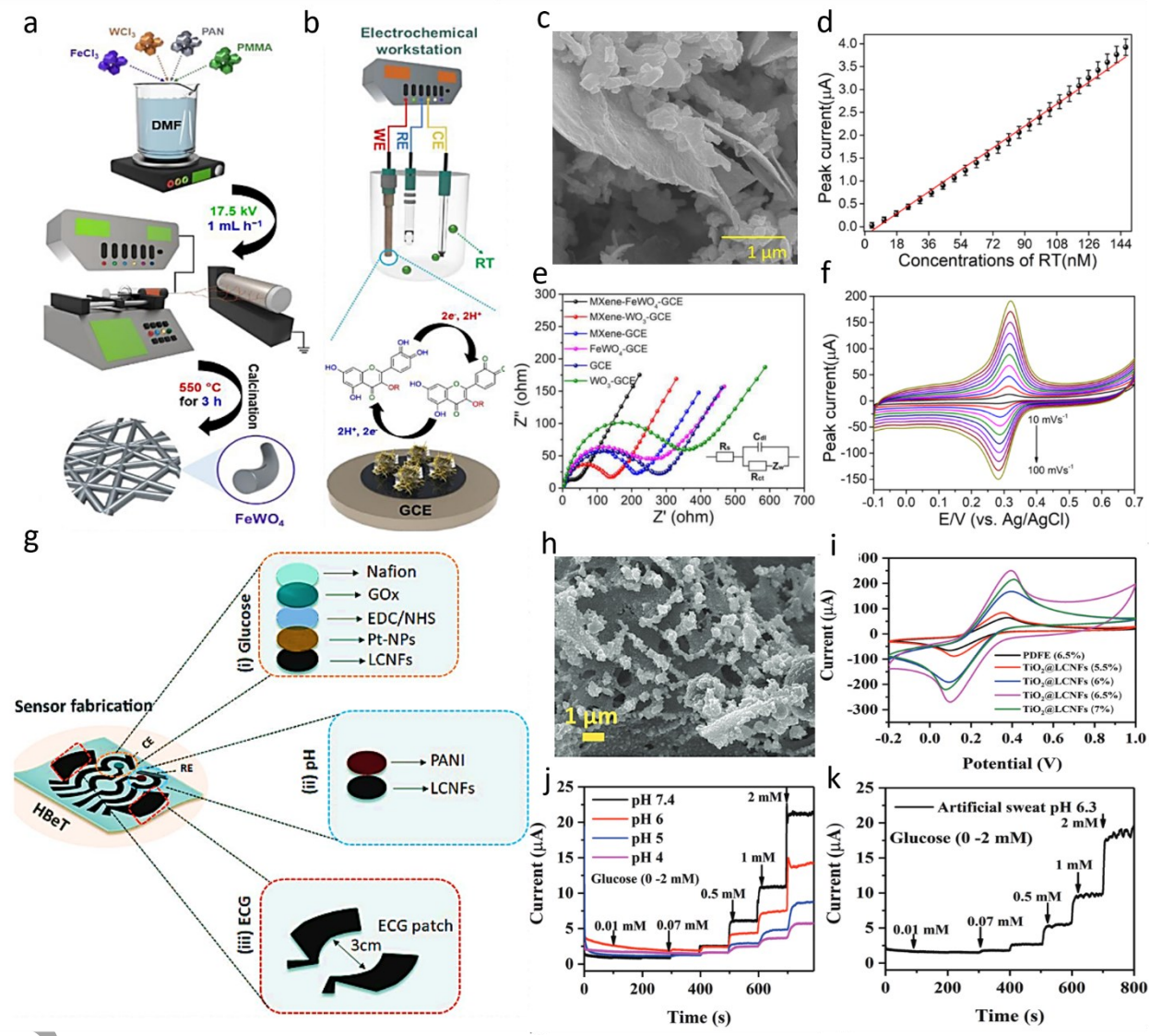

Figure 7. Characteristics of the MXene-$FeWO_4$ core-shell nanoarrays; (a) schematic illustration of the electrospinning procedure, (b) hybrid structure of the designed electrode, (c) SEM image, (d) calibration curve of the anodic current response against RT concentration, (e) Nyquist plot, and (f) CV curves in various scan rates. Reproduced from reference [123] with permission from Elsevier. Properties of MXene/fluoropolymer nanofiber loaded by TiO_2 nanoparticles; (g) the multiplexed hybrid sensor applications, (h) SEM image of the deposited TiO_2 on the deployed nanocomposite, (i) CV response of the designed nanofibers in 0.1 M KCl solution, (j) glucose biosensor calibration in various pHs, and (k) dynamic amperometry response in the pH of 6.3. Reproduced from reference [122] with permission from Wiley.

In another research, Ranjith et al. [123] reported the fabrication of $MnMoO_4$ nanofibers loaded with single-layered MXenes. The $MnMoO_4$ composite was used over a glassy carbon electrode (GCE) for hydroquinone (HQ) and catechol (CC) detection, known as two major toxic pollutants in wastewater. For preparing the electrospinning solution, $MnCl_2$, $MoCl_3$, polyacrylonitrile (PAN), and poly methyl methacrylate (PMMA) were dissolved in DMF. The appropriate nanofibers were fabricated under optimum conditions of 16.5 kV voltage, 1 ml h^{-1} feed rate, and 15 cm distance. Then, the collected nanofibrous mats were calcinated at 500°C for 3h with a 4°C.min^{-1} heating rate. In the next step, the MXene was functionalized using 3-mercaptopropionic acid and mixed with 100 mg $MnMoO_4$. The produced nanofibers were dispersed in ethanol, heated at 120°C for 6 h, centrifuged, and dried at 60°C. Finally, the $MnMoO_4$-Mxene composite was drop-casted over the GCE surface and dried. The presence of 2D MXene nanosheets in 1D $MnMoO_4$ nanofibers enhanced signal amplification and displayed electro-catalytic activity through the HQ and CC oxidation. Also, the designed composite depicted an oxidation potential of 0.203 V and 0.102 V for CC and HQ, respectively. The microscopic images illustrated the formation of bead-free nanofibers with 150 nm average diameter. Also, the HRTEM images illustrated the crystalline nature of the deployed composite with the lattice space of 0.34 nm, relating to the (220) plane of $MnMoO_4$. In addition, the structure with a 0.230 nm lattice spacing was attributed to the (103) MXene plane. The EIS evaluation was performed in 5 mM $[Fe(CN)_6]^{3-/4-}$ solution in the 1-100 MHz frequency range. The resistance values against electron transferring for bare GCE, MXene-GCE, $MnMoO_4$-GCE, and $MnMoO_4$-MXene-GCE were calculated approximately as 351, 239, 204, and 60 Ω, resulting from the Mn doping to the MoO-MXene-GCE which enhances conductivity and electro-catalytic capabilities. Moreover, the redox activity of the 10 µM of HQ and CC in 0.05 M PBS electrolyte was studied in the 2.0-9.0 pH range. CV evaluation displayed enhancing the anodic peak current by increasing the pH to 7.0. The fabricated biosensor might be protonated,

and –OH groups could be stabilized in the acidic condition (2.0-5.0). So, the pH=7.0 was recognized as the most stable condition for CC and HQ detection with high sensitivity. The repeatability RSD value of 3.12 and 1.84% were obtained for HQ and CC, respectively. Furthermore, the designed sensors were maintained for a month to investigate their electrochemical stability, retaining 92 and 94% of the peak current intensity for HQ and CC, respectively. Noteworthily, the sensors displayed a wide linear range of 5nM to 65 nM, as well as LOD of 0.26 nM and 0.3 nM for HQ and CC.

The future of electrochemical biosensors looks bright with the development of MXene-based microfluidic and wearable microfluidic biosensors. These biosensors are capable of detecting various biomarkers, such as proteins, nucleic acids, hormones, etc. They offer a reliable and safe wearable biosensing platform, as well as advanced microfluidic platforms for detecting very low-concentration biomolecules. They can track the wearer's health at a molecular level and address biofouling concerns. Meanwhile, some challenges need to be addressed in the next generation, such as low oxidative stability, non-scalable production, non-uniform surface termination, fluorine termination, surface defects, commercialization, and cytocompatibility. Also, point of care is an essential aspect of quick diagnosis, which is considered when constructing MXene-based biosensors. Scientists are exploring ways to combine the MXene surface groups with other biomolecules, such as antibodies and nucleic acids, to enhance their efficacy, while it should be noted that there have been only a few studies conducted on this so far.

7. MXene-loaded nanofibers for supercapacitor applications

Numerous research is being carried out on effective energy storage, specifically supercapacitors, in terms of increasing energy density (ED), power density (PD), cyclic stability, and fast charge-discharge. MXene materials, discovered by the group of Barsoum and Gogotsi [29], are a new class of materials that also find applications in energy storage i.e., supercapacitors. These Nanosheets have abundant active sites and conductivity (~2.6 × 10^3 S cm^{-1}) that participate in high and fast electron transport [124]. Additionally, their 2D structures facilitate fast electrolyte diffusion, and their functional groups help in rate capability enhancement. Meanwhile, the application of MXene in flexible and wearable electronics is limited due to its availability in powder form. Regarding the fabrication of flexible, binderless electrodes, electrospun nanofibers have been widely declared for future applications [125, 126]. Currently, the synthesis of the polymeric and carbonous nanofibers in combination with 2D MXene structures has been broadly explored toward approaching free-standing and flexible supercapacitor electrodes. MXene family has shown the pseudo-capacitive type of storage via an intercalation mechanism, resulting in extended electrochemical performance [127].

The research on MXene fibrous composite started with the introduction of MXene into the fibers followed by various processes, such as twisting, knitting, and weaving, which mighty result in the MXene detaching from the fibrous substrate, discontinuity, and so diminishing the conductivity [128, 129]. Additionally, the re-staking of MXene layers over fibrous layers can decrease the ion diffusion and result in final poor electrochemical performance. Therefore, MXene embedment into the nanofibers during the electrospinning procedure could be influential in addressing the obstacles mentioned above. In this view, Levitt et al. [13] prepared a high-performance supercapacitor electrode used as free-standing material without any binders and additives. In this attempt, a PAN-based nanofibrous mat containing 35 wt. % $Ti_3C_2T_x$ MXene was prepared using the facile electrospinning technique and carbonized to

obtain the carbon nanofiber/MXene composite mats. The designed composite exhibited a high capacitance of 205 mF cm^{-2} at 50 mV s^{-1}, three times superior to the bare carbon nanofibers. Also, they declared that the proposed composite could show better electrochemical performance than the PCL nanofibers integrated with the sprayed $Ti_3C_2T_x$ MXene.

Similarly, Hwang et al. [130] prepared the $Ti_3C_2T_x$ MXene/CNF composite using PAN as the precursor. In this work, they studied the impact of the MXene size on the characteristics of the synthesized fibers and their overall electrochemical performance. They have been categorized as small-(SMX), medium- (MMX), and large-sized MXene (LMX) with size ranges of 0.7-0.8, 2-3, and 6-8 μm, respectively. Microscopic images of the provided electrospun membranes are represented in **Figures 8a-c**. The CV curves at the scan rate of 300 mV s^{-1} illustrated a higher capacitance in the MXene-loaded specimens compared with the bare CNF, as shown in **Figure 8d**. SMX/CNF showed a high electrochemical performance with the lowest electrode and charge-transfer resistance compared to others. The reason could be attributed to the presence of higher mesoporosity, as well as MXene high metallic conductivity combined with the CNF network, preventing the filler aggregation and providing a stable network.

Using the same solution doping technique to obtain the flexible CNF-based electrodes, Yan et al. [131] combined PAN as a carbon source with Polyvinylpyrrolidone (PVP) as a sacrificial polymer to obtain porous CNFs (PCNFs). They added the Fe, Co, and MXene precursors into the PAN-PVP solution and electrospun to synthesize a nano fabric sheet. Then, the fabricated composite was furtherly stabilized and carbonized at 600°C to obtain the $FeCo_2O_4$/MXene/PCNF membrane. The $FeCo_2S_4$/MXene/PCNF flexible hybrid film was then attained by subjecting the prepared film to a hydrothermal procedure in the presence of Thioacetamide (TAA). The $FeCo_2S_4$/MXene/PCNF membrane inherited a 3D pore construction, containing hierarchical PCNF nanostructure. Accordingly, a surface area of 176.8

$m^2.g^{-1}$ and an excellent electrical conductivity of 1.2 S cm^{-1} were obtained. The porous nanostructure could create pathways for rapid diffusion of the applied electrolyte, thus gaining electrochemically active nanostructures of $FeCo_2S_4$. Additionally, CNFs could play the role of a conductive core, facilitating the transport of electrons, fast $FeCo_2S_4$ sheath redox reaction, and long-term durability. The attached MXene nanosheets to the $FeCo_2S_4$ compound provided admirable electrical conductivity and plentiful edge sites, promoted rapid reaction kinetics, declined the $FeCo_2S_4$ volume expansion, and improved electrochemical performance. The designed asymmetric supercapacitor device, comprising the PCNF negative electrode and $FeCo_2S_4$/MXene/PCNF positive electrode, yielded an ED of 86.7 Wh kg^{-1} at a PD of 800 W kg^{-1}.

In another study, Chen et al. [124] prepared a composite using commercial carboxymethylated CNF with the $Ti_3C_2T_x$ MXene and Porous Carbon (PC). They designed the hybrid film of the material using the vacuum-filtration method. In the proposed structure, PC could fulfill the porosity requirement for charge storage and fast ion diffusion. 2D $Ti_3C_2T_x$ offered a high conductivity of 2.6×10^3 $S.cm^{-1}$ and a proper film-forming capability. The one-dimensional CNF structure ensured proper mechanical characteristics with a great tensile strength of 38.6 MPa via binding of the adjacent $Ti_3C_2T_x$ flakes and PC. Also, they explored the promising role of the designed flexible composite film as an electrode in a quasi-solid-state supercapacitor and demonstrated appropriate electrochemical performance with high flexibility.

Direct growth of a highly porous structure onto conducting MXene-CNF composite can further enhance the ED and PD of the device to several folds due to more charge accommodation. Recently, Kshetri et al. [132] reported a complex composite structure prepared by growing the Co-MOF having spikes morphology over the surface of MXene-CNFs. As such CNF showed an average diameter of 201 ± 19 nm, which increased to 350 ± 23 nm after embedding MXene

filler. The Co-MOF was used in this attempt to gain a metal-loaded PC using a heat treatment process. So, Co-MOF@MXene-CNF composite fibers were further carbonized at 900°C to provide a Co-PC@MXene-CNF structure with a high surface area of 268 $m^2 g^{-1}$. The flexible solid-state device consists of Co-PC@MX-CNF, MnO_2@Co_3O_4-PC@MXene-CNF, and PVA/KOH, respectively, as negative and positive electrodes, and the quasi-solid-state electrolyte figured out an ED of 72.5 Wh kg^{-1} at a PD of 832.4 W kg^{-1}. Also, it could endure an ED of 37.1 Wh kg^{-1} at a PD of 15000 W kg^{-1}. A green LED could be light up through connecting two designed devices in series for up to 21 minutes continuously. In another approach, ZIF-67-loaded MXene/PAN nanofibers were designed [134]. They grew ZIF-67 cubic shape over MXene/PAN nanofibers and then stabilized (250°C) and carbonized (700°C) it to get highly mesoporous MXene-loaded CNFs. **Figure 8e** shows a schematic of the synthesis procedure used in this exploration. FESEM images of the specimens before and after the carbonization procedure are also depicted in **Figures 8f&g**. These nanofibers showed a type IV adsorption-desorption hysteresis with a surface area of 405.9 m^2 g^{-1}. The specific capacitance of 572.7 F g^{-1} was achieved at 1 Ag^{-1} with cyclic stability of 96.4% after 10,000 cycles (see **Figure 8h**). CV curves of the samples at several scan rates in the symmetric and asymmetric devices are also represented in **Figures 8i&j**. The flexibility of the electrode concerning its electrochemical performance was tested by bending it at 60° and 90°, as well as twisting it during CV and GCD cycles. The coinciding curves at different bending positions displayed the remarkable flexibility of the designed solid-state device with an ED of 22.53 Wh kg^{-1} at a PD of 499.9W kg^{-1}. In the case of the assembled asymmetric device using a fabricated electrode as a positive and a Co_3O_4/Ni foam as the negative electrode, a superior ED of 74.2 Wh kg^{-1} was achieved at 800 W kg^{-1} PD.

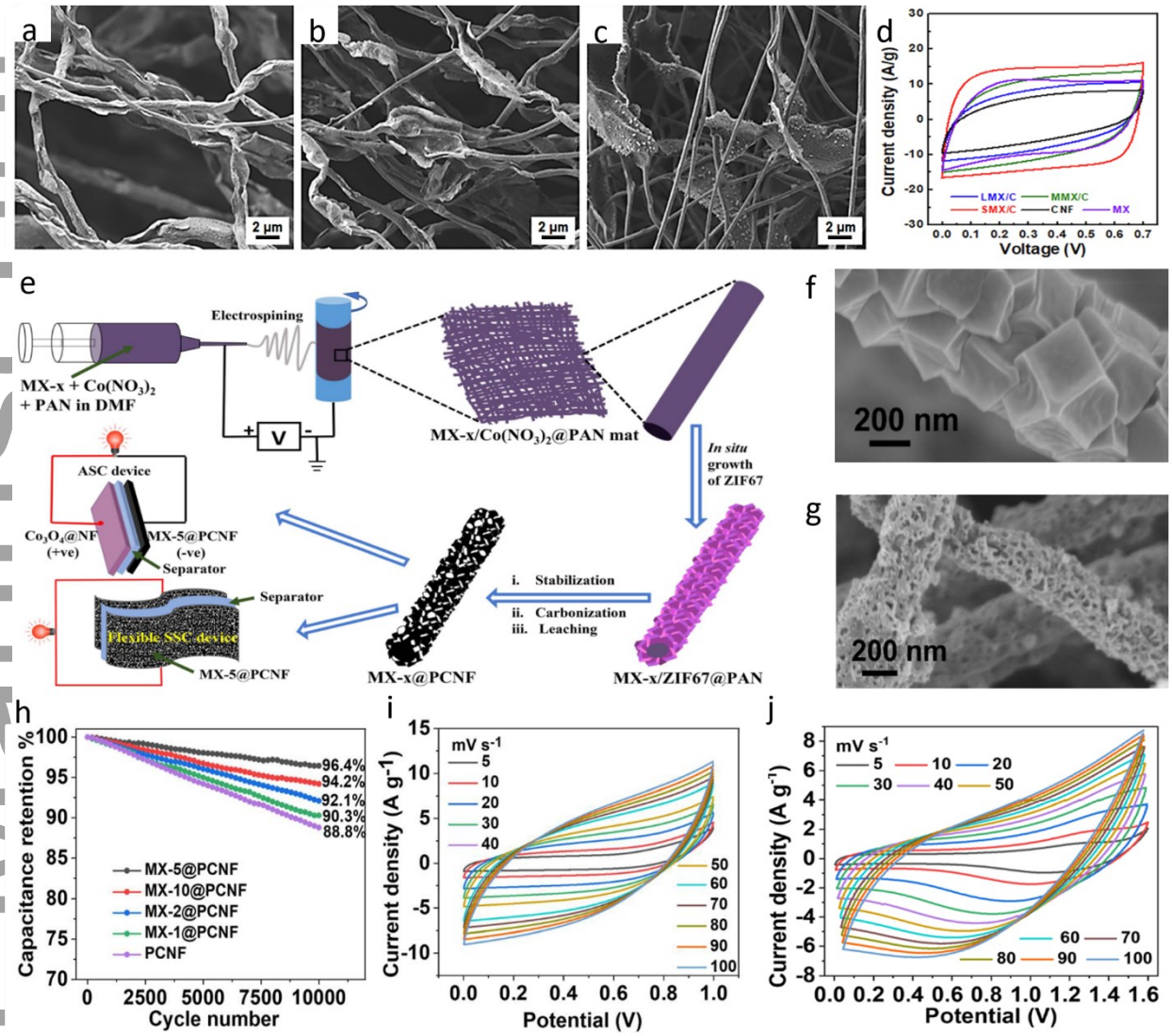

Figure 8. Characteristics of the PAN-based CNF loaded by MXene nanosheets with various sizes, including 0.7-0.8 (SMX), 2-3 (MMX), and 6-8 μm (LMX); (a-c) SEM images of the samples integrated with SMX, MMX, and LMX, respectively, and (d) CV curves of the electrospun samples with a scan rate of 300 mV s^{-1}. Reproduced from reference [130] with permission from Elsevier. Features of the MXene/PAN nanofibers embedded with ZIF-67; (e) schematic illustration of the synthesis procedure, (f) FESEM image of the MXene/ZIF-67 on PAN nanofibers, (g) FESEM image of the MXene/ZIF-67 on CNF, (h) cycling stability performance (i) CV curves in a symmetric device at various scan rates, and (j) CV curves at different scan rates in an asymmetric device. Reproduced from reference [134] with permission from the Royal Society of Chemistry.

Donthula et al. [135] also fabricated ternary composite material, consisting of RuO_2, MXene, and CNFs by a direct spinning method. $RuCl_2$ and MXene delaminated sheets were dispersed in PAN solution followed by an electrospinning step at 15 kV electric voltage, 10 cm distance, and 1 ml h^{-1} flow rate. Stabilization (250°C) and Carbonization (900°C) processes were performed on the ternary composite. RuO_2 could be effective in charge storing by the pseudocapacitive mechanism, while MXene layers stored charge through a faradic reaction, as well as intercalation of electrolyte ions. The prepared electrode for the composite could deliver a capacitance of 322 F g^{-1} at 1 Ag^{-1}. This material also depicted a good rate capability (62.9%) and retained 90% of the capacity after 2500 cycles. The bending and restoring exercises were performed to conform to the electrode flexibility. Instead of electrospinning, a wet spinning method followed by coagulation was adopted to embed higher MXene concentrations up to 80% [136], leading to the highest porosity with a surface area of 550.25 m^2 g^{-1}. Additionally, it was figured out that the area under the CV curve could increase with the rise in MXene loading. The suggested fibrous composite showed a high areal capacitance of 2160 mF cm^{-2} at 3.86 mA cm^{-2} in the potential range of -1 to 0 V. In addition, a capacitance of 1421.06 mF cm^{-2} at a current density of 3.86 mA cm^{-2} in positive voltage of 0 to 0.5 V was observed through the $NiCo_2S_4$ addition. They also developed a fiber-shaped supercapacitor device with $NiCo_2S_4$ sheet arrays electrodeposited over MXene-CFs as negatrodes. The specific capacitance obtained in this case was 939.18 mF cm^{-2} at 3.09 mA cm^{-2}. Furthermore, the asymmetric device possessed a volumetric ED of 40.70 mWh cm^{-3} at a PD of 301.51 mW cm^{-3}. **Table 2** summarizes more attempts carried out in this area.

Table 2. The advancement of electrospun-based supercapacitors integrated with MXene nanosheets.

Designed structure	Outcome	Performance	Ref.
Flexible nitrogen-doped porous MXene nanofibers	-The provided porous structure diminished restacking of the MXene nanoflakes. -Redox reactivity, as well as electron transport of the MXene nanosheets were enhanced, resulting from the presence of nitrogen atoms. -High specific surface area, along with more active sites provided higher electrochemical performances.	12.78 Wh kg^{-1} energy density and 1080 W kg^{-1} power density up to 5000 cycles	[137]
Co_9S_8 hollow core structure coated with MXene and Bi_2O_3 shells	-The presence of MXene and Bi_2O_3 led to attesting frequent electroactive sites and so improved conductivity for supplying desirable rate of capacity.	High discharge capacitance of 646.1 F g^{-1} at 1 Ag^{-1}, along with high stability after 5000 cycles	[138]
Decorated MXene/carbon nanofiber core-shell structure with polypyrrole layer	-Inherent conductivity and electrochemical features of MXene improved electronic movement. -The conductivity and pseudocapacitive activity were enhanced with the delocalized π-electrons in the polypyrrole structure.	The energy density of 61.3 Wh kg^{-1} at a 796.8 W kg^{-1} power density and 92.8% capacitance retention after 10,000 cycles	[139]
Porous carbon nanofibers integrated with $Ti_3C_2T_x$ MXene nanosheets	-Surface terminating groups of MXenes could boost the performance via acting as a pseudocapacitance. -The capacitance increased through the addition of MXene up to 5%, while further addition caused adverse results, mighty due to particle agglomeration and reduction of the channels.	Energy density of 22.53 Wh kg^{-1} and 96.4% capacitance retention after 10 000 cycles	[133]

MXene/cellulose nanofibers	-The proper electrochemical activity obtained could be linked with the strong interaction between MXene nanosheets and cellulose nanofibrous substrate, ensuring the MXene alignment structure during bending and high stability against mechanical deformation.	The specific capacitance of 93.9 mF cm^{-2} at a 0.1 mA cm^{-2} current density and 87% capacitance retention at 2 mA cm^{-2} after 5000 cycles	[140]
$Ti_3C_2T_x$/polyaniline nanofibers	-Polyaniline nanofibers were incorporated between the MXene layers, providing bridges for feasible ion transferring. -The electrolyte ion diffusion was favored, resulting from the frequent active sites, as well as high specific surface area.	The high capacitance of 645.7 F g^{-1} and 98% capacitance retention after 5000 cycles	[141]
MXene/carbon nanofibers covered by RuO_x	-The RuO_x layer was easily coated on the carbon nanofibers due to the abundant functional groups on the MXene nanosheets. -The coating layer improved the wettability and resulted in boosting the charge transport.	The energy density of 8.5 Wh kg^{-1} at 85.8 W kg^{-1} power density and 99% capacitance retention after 10,000 cycles	[142]

Even though there are other MXene versions made of various transition metal carbides and nitrides, $Ti_3C_2T_x$ is the only one that has been studied for use in flexible supercapacitor applications. Till now, MXene-nanofiber materials are less explored and need apposite consideration and optimization for viable industrial applications. Further, the MXene materials could be functionalized (heteroatom doping) to bond with CNFs, which will not only advance the electrochemical charge transfer but also boost the mechanical strength. The adoption of biopolymers in place of synthetic polymers will cut costs and environmental impacts even more. MXene intercalation engineering with suitable atoms is one of the imperative aspects to improve electrochemical activity synergistically. Notably, researchers should be aware of

potential restrictions linked with the MXene architectures that may affect their application in supercapacitor devices. Limited energy density, relatively low volumetric capacity, non-even intercalation of ions into all types of MXene layers, sensitivity to environmental factors, and fabrication complexity compared to advanced substances are assumed have remained sluggish yet. Furthermore, ensuring compatibility and optimal performance with other supercapacitor components, such as electrolytes and electrodes, may require additional research and customization efforts.

8. Future Outlook

The MXene exploration continues to enlarge the knowledge boundaries, especially in the field of electrochemical and electroactive devices. For the future, more attention is suggested to optimize the MXene synthesis procedure, modify terminational groups on their surfaces, maximize their overall merits, and systematically develop green and eco-friendly fabrication routes. In addition, $Ti_3C_2T_x$ is frequently employed in research in this era, while far too little attention has been paid to other MXene structures, which are recommended to be evaluated. Also, it is essential to deploy systematic research and development techniques to enhance MXene stability. Moreover, the homogeneity of MXene layers, as well as their morphology, should be manipulated. Regarding the MXene/nanofiber composites, the fabrication of biopolymers or waste materials as the fiber's precursors should be envisioned to approach green and eco-friendly electrochemical devices. As electrospun fibers have faced poor mechanical strength in electrochemical tools, the engineering of the electrospun fibers with other 3D printed, electro-written, or film layers as hybrid integrated layouts should be brought into force. Furthermore, the effect of MXene-based composites on human health and the environment is supposed to be investigated due to the potential presence of metallic atoms. The

production, use, and eventual disposal of MXene-based devices should be scrutinized for their environmental impact. This encompasses both the material itself and any by-products or waste generated during manufacturing and end-of-life scenarios. In terms of future perspective, the recycling ability of the MXene and maintaining its inherent features after the recycling process should also be focused on. For commercializing and mass production of the MXene-loaded electrospun networks, the electrochemical performances of these electrochemical devices should be boosted. It is also suggested to deploy flexible and wearable devices with multifunctional applications. **Figure 9** renders the outlook regarding the electrospun fibers embedded with MXene nanosheets as various electrochemical tools. Overall, the decorated miniaturized fibers with the MXene hybrid layers could be a promising candidate for commercializing self-reliant electrochemical devices after further resolving the adverse issues.

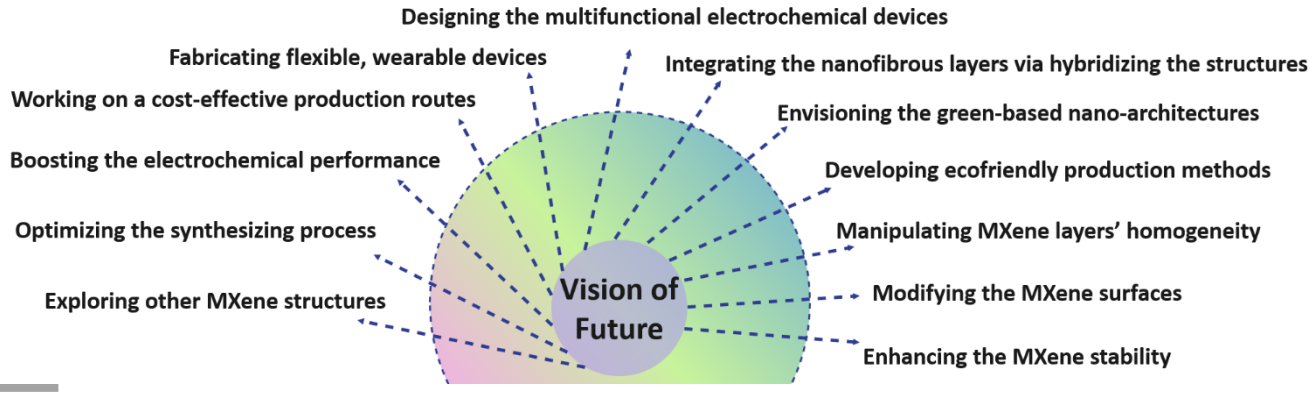

Figure 9. Future perspectives of the electrospun electrochemical devices incorporated with MXene nanosheets.

9. Conclusion

Electrochemical technology is a key building block to diminish pollution, fossil fuel depletion, and environmental impairment. Additionally, it is considered a crucial element for technology growth, healthcare monitoring, hindering human disabilities, cost reduction, and so forth. Today, an exceptional range of 2D nanomaterials has been introduced to enhance the

performance of electrochemical devices. Since 2011, many efforts have been conducted to characterize the MXene lamellar structure, showing superior electrical conductivity, mechanical robustness, hydrophilicity, intercalation characteristics, optical features, and thermal properties, as well as adjustable surface terminations and easy functionalization over other typical nanostructures. Meanwhile, several drawbacks have been declared for the bare MXene family, including detaching from the substrate, agglomeration, delamination of their layers, and oxidizing-related degradation, which are required to be addressed. A potential strategy to address these shortcomings could be MXene direct embedding into the miniaturized fibers fabricated through the electrospinning system. Despite many evaluations of the usage of MXene-loaded nanofibers, exploring their applications in electrochemical devices is still in the infant stage. Accordingly, synthesis methods, as well as characteristics of the MXene architectures, were reviewed in this paper. Then, the fabrication and behavior of the electrospun fibers loaded by the MXene nanosheets were highlighted in the actuator, battery, fuel cell, sensor, and supercapacitor electrochemical devices. Correspondingly, this review remarked on influential paths to obtain the synergetic effects of the MXene layers and electrospun fibers in various electrochemical devices, implying outstanding electrochemical performance in targeted power tools.

Acknowledgment

YKM acknowledges the funding by Interreg Deutschland–Denmark with money from the European Regional Development Fund, project number 096-1.1-18 (Access and Acceleration), from the ESS lighthouse on hard materials in 3D, SOLID (Danish Agency for Science and Higher Education, grant number 8144-00002B), from BHJ Fonden and Fabrikant Mads Clausen Fonden, Denmark.

Author Contributions

SNB: Conceptualization, analysis, investigation, methodology, resources, supervision, writing original draft. SK: Conceptualization, analysis, investigation, resources, supervision, writing original draft. AG, NP, AAG, VVJ, WUA, MS, MB, EC: Analysis, investigation, methodology, resources, supervision, writing original draft, revision. YKM: Conceptualization, analysis, investigation, methodology, resources, supervision, writing original draft and revision.

References

1. Chamanehpour, E.; Sayadi, M. H.; Hajiani, M., *Advanced Composites and Hybrid Materials* **2022,** *5* (3), 2461-2477.
2. Zhao, Y.; Song, Z.; Li, X.; Sun, Q.; Cheng, N.; Lawes, S.; Sun, X., *Energy storage materials* **2016,** *2*, 35-62.
3. Chamanehpour, E.; Sayadi, M. H.; Hajiani, M., *Journal of Photochemistry and Photobiology A: Chemistry* **2023,** *434*, 114221.
4. Zhu, C.-y.; Ye, Y.-w.; Guo, X.; Cheng, F., *New Carbon Materials* **2022,** *37* (1), 59-92.
5. Solangi, N. H.; Karri, R. R.; Mazari, S. A.; Mubarak, N. M.; Jatoi, A. S.; Malafaia, G.; Azad, A. K., *Coordination Chemistry Reviews* **2023,** *477*, 214965.
6. Zhong, Q.; Li, Y.; Zhang, G., *Chemical Engineering Journal* **2021,** *409*, 128099.
7. Zhan, X.; Si, C.; Zhou, J.; Sun, Z., *Nanoscale Horizons* **2020,** *5* (2), 235-258.
8. Gao, L.; Li, C.; Huang, W.; Mei, S.; Lin, H.; Ou, Q.; Zhang, Y.; Guo, J.; Zhang, F.; Xu, S., *Chemistry of Materials* **2020,** *32* (5), 1703-1747.
9. Jimmy, J.; Kandasubramanian, B., *European Polymer Journal* **2020,** *122*, 109367.
10. Orangi, J.; Hamade, F.; Davis, V. A.; Beidaghi, M., *ACS nano* **2019,** *14* (1), 640-650.
11. Yang, W.; Yang, J.; Byun, J. J.; Moissinac, F. P.; Xu, J.; Haigh, S. J.; Domingos, M.; Bissett, M. A.; Dryfe, R. A.; Barg, S., *Advanced materials* **2019,** *31* (37), 1902725.
12. De Lama-Odría, M. d. C.; del Valle, L. J.; Puiggalí, J., Melt Electrospinning and Electrowriting for Pharmaceutical and Biomedical Applications. In *Nano-and Microfabrication Techniques in Drug Delivery: Recent Developments and Future Prospects*, Springer: 2023; pp 41-70.
13. Levitt, A. S.; Alhabeb, M.; Hatter, C. B.; Sarycheva, A.; Dion, G.; Gogotsi, Y., *Journal of Materials Chemistry A* **2019,** *7* (1), 269-277.
14. Banitaba, S. N.; Ebadi, S. V.; Salimi, P.; Bagheri, A.; Gupta, A.; Arifeen, W. U.; Chaudhary, V.; Mishra, Y. K.; Kaushik, A.; Mostafavi, E., *Materials Horizons* **2022,** *9* (12), 2914-2948. DOI 10.1039/D2MH00879C.
15. Elham. Chamanehpour, S. T., Horst-Günter. Rubahn, Alireza. Dolatshahi-Pirouz, Yogendra Kumar. Mishra, *Advanced Materials Technologies* **2023**, 2301392. DOI https://doi.org/10.1002/admt.202301392.
16. Khademolqorani, S.; Zeinal Hamadani, A.; Tavanai, H., *Journal of Nanoparticles* **2014,** *2014*.
17. Shi, S.; Si, Y.; Han, Y.; Wu, T.; Iqbal, M. I.; Fei, B.; Li, R. K.; Hu, J.; Qu, J., *Advanced Materials* **2022,** *34* (17), 2107938.
18. Zhang, Y.; Zhang, X.; Silva, S. R. P.; Ding, B.; Zhang, P.; Shao, G., *Advanced Science* **2022,** *9* (4), 2103879.
19. Banitaba, S. N.; Semnani, D.; Heydari-Soureshjani, E.; Arifeen, W. U.; Ko, T. J.; Rezaei, B.; Ensafi, A. A.; Latifi, M.; Mostafavi, E.; Kaushik, A., *Journal of Alloys and Compounds* **2022,** *924*, 166482.
20. Banitaba, S. N.; Semnani, D.; Heydari-Soureshjani, E.; Arifeen, W. U.; Ko, T. J.; Rezaei, B.; Ensafi, A. A.; Latifi, M.; Mostafavi, E.; Kaushik, A. K., *ACS Applied Energy Materials* **2023**.
21. Bashir, T.; Zhou, S.; Yang, S.; Ismail, S. A.; Ali, T.; Wang, H.; Zhao, J.; Gao, L., *Electrochemical Energy Reviews* **2023,** *6* (1), 5. DOI 10.1007/s41918-022-00174-2.
22. Xu, Z.; Deng, W.; Wang, X., *Electrochemical Energy Reviews* **2021,** *4* (2), 269-335. DOI 10.1007/s41918-021-00094-7.
23. Banitaba, S. N.; Khademolqorani, S.; Jadhav, V. V.; Mishra, Y. K.; Mostafavi, E.; Kaushik, A., *Materials Today Electronics* **2023**, 100055.
24. Sobolčiak, P.; Ali, A.; Hassan, M. K.; Helal, M. I.; Tanvir, A.; Popelka, A.; Al-Maadeed, M. A.; Krupa, I.; Mahmoud, K. A., *PLoS One* **2017,** *12* (8), e0183705.
25. Wang, H.; Sun, C.; Cao, Y.; Zhu, J.; Chen, Y.; Guo, J.; Zhao, J.; Sun, Y.; Zou, G., *Carbon* **2017,** *114*, 628-634. DOI https://doi.org/10.1016/j.carbon.2016.12.081.

26. Yuan, W.; Yang, K.; Peng, H.; Li, F.; Yin, F., *Journal of Materials Chemistry A* **2018,** *6* (37), 18116-18124.
27. Guo, Y.; Zhang, D.; Yang, Y.; Wang, Y.; Bai, Z.; Chu, P. K.; Luo, Y., *Nanoscale* **2021,** *13* (8), 4624-4633. DOI 10.1039/D0NR09228B.
28. Wu, S.; Luo, H.; Shen, W.; Su, J.; Ma, C.; Wu, J., *Materials Letters* **2022,** *314*, 131922.
29. Naguib, M.; Kurtoglu, M.; Presser, V.; Lu, J.; Niu, J.; Heon, M.; Hultman, L.; Gogotsi, Y.; Barsoum, M. W., *Advanced materials* **2011,** *23* (37), 4248-4253.
30. Novoselov, K. S.; Geim, A. K.; Morozov, S. V.; Jiang, D.-e.; Zhang, Y.; Dubonos, S. V.; Grigorieva, I. V.; Firsov, A. A., *science* **2004,** *306* (5696), 666-669.
31. Wang, Q. H.; Kalantar-Zadeh, K.; Kis, A.; Coleman, J. N.; Strano, M. S., *Nature nanotechnology* **2012,** *7* (11), 699-712.
32. Zhong, Y.; Xia, X.; Shi, F.; Zhan, J.; Tu, J.; Fan, H. J., *Advanced Science (Weinheim, Baden-wurttemberg, Germany)* **2017,** *4* (3), 201700047-201700047.
33. Gogotsi, Y. G.; Andrievski, R. A., *Materials science of carbides, nitrides and borides*. Springer Science & Business Media: **2012**; Vol. 68.
34. Kang, Z.; Khan, M. A.; Gong, Y.; Javed, R.; Xu, Y.; Ye, D.; Zhao, H.; Zhang, J., *Journal of Materials Chemistry A* **2021,** *9* (10), 6089-6108.
35. Anasori, B.; Lukatskaya, M. R.; Gogotsi, Y., *Nature Reviews Materials* **2017,** *2* (2), 1-17.
36. Mashtalir, O.; Naguib, M.; Mochalin, V. N.; Dall'Agnese, Y.; Heon, M.; Barsoum, M. W.; Gogotsi, Y., *Nature communications* **2013,** *4* (1), 1716.
37. Vasyukova, I. A.; Zakharova, O. V.; Kuznetsov, D. V.; Gusev, A. A., *Nanomaterials* **2022,** *12* (11), 1797.
38. Naguib, M.; Come, J.; Dyatkin, B.; Presser, V.; Taberna, P.-L.; Simon, P.; Barsoum, M. W.; Gogotsi, Y., *Electrochemistry Communications* **2012,** *16* (1), 61-64.
39. Naguib, M.; Barsoum, M. W.; Gogotsi, Y., *Advanced Materials* **2021,** *33* (39), 2103393.
40. Shuck, C. E.; Sarycheva, A.; Anayee, M.; Levitt, A.; Zhu, Y.; Uzun, S.; Balitskiy, V.; Zahorodna, V.; Gogotsi, O.; Gogotsi, Y., *Advanced Engineering Materials* **2020,** *22* (3), 1901241.
41. Kumar, J. A.; Prakash, P.; Krithiga, T.; Amarnath, D. J.; Premkumar, J.; Rajamohan, N.; Vasseghian, Y.; Saravanan, P.; Rajasimman, M., *Chemosphere* **2022,** *286*, 131607.
42. Mashtalir, O.; Naguib, M.; Dyatkin, B.; Gogotsi, Y.; Barsoum, M. W., *Materials Chemistry and Physics* **2013,** *139* (1), 147-152.
43. Ling, Z.; Ren, C. E.; Zhao, M.-Q.; Yang, J.; Giammarco, J. M.; Qiu, J.; Barsoum, M. W.; Gogotsi, Y., *Proceedings of the National Academy of Sciences* **2014,** *111* (47), 16676-16681.
44. Alhabeb, M.; Maleski, K.; Anasori, B.; Lelyukh, P.; Clark, L.; Sin, S.; Gogotsi, Y., *Chemistry of Materials* **2017,** *29* (18), 7633-7644.
45. Driscoll, N.; Richardson, A. G.; Maleski, K.; Anasori, B.; Adewole, O.; Lelyukh, P.; Escobedo, L.; Cullen, D. K.; Lucas, T. H.; Gogotsi, Y., *Acs Nano* **2018,** *12* (10), 10419-10429.
46. Ghidiu, M.; Lukatskaya, M. R.; Zhao, M.-Q.; Gogotsi, Y.; Barsoum, M. W., *Nature* **2014,** *516* (7529), 78-81.
47. Lukatskaya, M. R.; Mashtalir, O.; Ren, C. E.; Dall'Agnese, Y.; Rozier, P.; Taberna, P. L.; Naguib, M.; Simon, P.; Barsoum, M. W.; Gogotsi, Y., *Science* **2013,** *341* (6153), 1502-1505.
48. Sun, W.; Shah, S.; Chen, Y.; Tan, Z.; Gao, H.; Habib, T.; Radovic, M.; Green, M., *Journal of Materials Chemistry A* **2017,** *5* (41), 21663-21668.
49. Zhou, C.; Zhao, X.; Xiong, Y.; Tang, Y.; Ma, X.; Tao, Q.; Sun, C.; Xu, W., *European Polymer Journal* **2022**, 111063.
50. Ashraf, I.; Ahmad, S.; Nazir, F.; Dastan, D.; Shi, Z.; Garmestani, H.; Iqbal, M., *International Journal of Hydrogen Energy* **2022,** *47* (64), 27383-27396.
51. He, H.; Wang, J.; Xia, Q.; Wang, L.; Hu, Q.; Zhou, A., *Applied Surface Science* **2021,** *568*, 150971.
52. Saha, S.; Arole, K.; Radovic, M.; Lutkenhaus, J. L.; Green, M. J., *Nanoscale* **2021,** *13* (39), 16543-16553.
53. Kamysbayev, V.; Filatov, A.; Hu, H.; Rui, X.; Lagunas, F., *Science* **2020,** *369*, 979-983.

54. Ming, F.; Liang, H.; Huang, G.; Bayhan, Z.; Alshareef, H. N., *Advanced Materials* **2021,** *33* (1), 2004039.
55. Naguib, M.; Halim, J.; Lu, J.; Cook, K. M.; Hultman, L.; Gogotsi, Y.; Barsoum, M. W., *Journal of the American Chemical Society* **2013,** *135* (43), 15966-15969.
56. Xu, X.; Yang, L.; Zheng, W.; Zhang, H.; Wu, F.; Tian, Z.; Zhang, P.; Sun, Z., *Materials Reports: Energy* **2022**, 100080.
57. Cheng, N.; Zhang, L.; Doyle-Davis, K.; Sun, X., *Electrochemical Energy Reviews* **2019,** *2*, 539-573.
58. Bai, X.; Guan, J., *Chinese Journal of Catalysis* **2022,** *43* (8), 2057-2090.
59. Kalambate, P. K.; Gadhari, N. S.; Li, X.; Rao, Z.; Navale, S. T.; Shen, Y.; Patil, V. R.; Huang, Y., *TrAC Trends in Analytical Chemistry* **2019,** *120*, 115643.
60. Zhang, B.; Boretti, A.; Castelletto, S., *Chemical Engineering Journal* **2022**, 134959.
61. Chang, H.; Li, X.; Shi, L.; Zhu, Y.-R.; Yi, T.-F., *Chemical Engineering Journal* **2021,** *421*, 129944.
62. Yang, L.; Cui, J.; Zhang, L.; Xu, X.; Chen, X.; Sun, D., *Advanced Functional Materials* **2021,** *31* (27), 2101378.
63. Pang, D.; Alhabeb, M.; Mu, X.; Dall'Agnese, Y.; Gogotsi, Y.; Gao, Y., *Nano Letters* **2019,** *19* (10), 7443-7448.
64. Ilango, P. R.; Savariraj, A. D.; Huang, H.; Li, L.; Hu, G.; Wang, H.; Hou, X.; Kim, B. C.; Ramakrishna, S.; Peng, S., *Electrochemical Energy Reviews* **2023,** *6* (1), 12. DOI 10.1007/s41918-022-00148-4.
65. Nitta, N.; Wu, F.; Lee, J. T.; Yushin, G., *Materials today* **2015,** *18* (5), 252-264.
66. Manthiram, A., *ACS central science* **2017,** *3* (10), 1063-1069.
67. Chen, T.; Jin, Y.; Lv, H.; Yang, A.; Liu, M.; Chen, B.; Xie, Y.; Chen, Q., *Transactions of Tianjin University* **2020,** *26* (3), 208-217.
68. Li, H., *Joule* **2019,** *3* (4), 911-914.
69. Tao, R.; Zhang, T.; Tan, S.; Jafta, C. J.; Li, C.; Liang, J.; Sun, X. G.; Wang, T.; Fan, J.; Lu, Z., *Advanced Energy Materials* **2022,** *12* (36), 2200519.
70. Salimi, P.; Tieuli, S.; Taghavi, S.; Venezia, E.; Fugattini, S.; Lauciello, S.; Prato, M.; Marras, S.; Li, T.; Signoretto, M., *Green Chemistry* **2022,** *24* (10), 4119-4129.
71. Larcher, D.; Tarascon, J.-M., *Nature chemistry* **2015,** *7* (1), 19-29.
72. Mahmud, S.; Rahman, M.; Kamruzzaman, M.; Ali, M. O.; Emon, M. S. A.; Khatun, H.; Ali, M. R., *Results in Engineering* **2022**, 100472.
73. Fichtner, M.; Edström, K.; Ayerbe, E.; Berecibar, M.; Bhowmik, A.; Castelli, I. E.; Clark, S.; Dominko, R.; Erakca, M.; Franco, A. A., *Advanced Energy Materials* **2022,** *12* (17), 2102904.
74. Xu, Y.; Dong, K.; Jie, Y.; Adelhelm, P.; Chen, Y.; Xu, L.; Yu, P.; Kim, J.; Kochovski, Z.; Yu, Z., *Advanced Energy Materials* **2022,** *12* (19), 2200398.
75. Das, P.; Wu, Z.-S., *Journal of Physics: Energy* **2020,** *2* (3), 032004.
76. Jyoti, J.; Singh, B. P.; Sandhu, M.; Tripathi, S. K., *Sustainable Energy & Fuels* **2022,** *6* (4), 971-1013.
77. Aghamohammadi, H.; Eslami-Farsani, R.; Castillo-Martinez, E., *Journal of Energy Storage* **2022,** *47*, 103572.
78. Tang, Q.; Zhou, Z.; Shen, P., *Journal of the American Chemical Society* **2012,** *134* (40), 16909-16916.
79. Luan, S.; Han, M.; Xi, Y.; Wei, K.; Wang, Y.; Zhou, J.; Hou, L.; Gao, F., *Ionics* **2020,** *26*, 51-59.
80. Greaves, M.; Barg, S.; Bissett, M. A., *Batteries & Supercaps* **2020,** *3* (3), 214-235.
81. Zhang, T.; Zhang, L.; Hou, Y., *eScience* **2022**.
82. Xu, H.; Zheng, D.; Liu, F.; Li, W.; Lin, J., *Journal of Materials Chemistry A* **2020,** *8* (12), 5853-5858.
83. Hu, B.; Kuang, X.; Xu, S.; Wang, X. In *A novel strategy for lithium-ion battery anode with enhanced cycling performance: silicon particles enclosed in shell-like MXenes/CNTs nanostructure*,

2019 IEEE 32nd International Conference on Micro Electro Mechanical Systems (MEMS), IEEE: **2019**; pp 946-949.
84. Wu, Y.; Sun, Y.; Zheng, J.; Rong, J.; Li, H.; Niu, L., *Journal of Physics: Energy* **2021,** *3* (3), 032009.
85. Nan, J.; Guo, X.; Xiao, J.; Li, X.; Chen, W.; Wu, W.; Liu, H.; Wang, Y.; Wu, M.; Wang, G., *Small* **2021,** *17* (9), 1902085.
86. Ma, Q.; Zhang, Z.; Kou, P.; Wang, D.; Wang, Z.; Sun, H.; Zheng, R.; Liu, Y., *Journal of Colloid and Interface Science* **2022,** *617*, 147-155.
87. Bhat, A.; Anwer, S.; Bhat, K. S.; Mohideen, M. I. H.; Liao, K.; Qurashi, A., *npj 2D Materials and Applications* **2021,** *5* (1), 61.
88. Tariq, H. A.; Nisar, U.; Abraham, J. J.; Ahmad, Z.; AlQaradawi, S.; Kahraman, R.; Shakoor, R., *Applied Surface Science* **2022,** *583*, 152441.
89. Seo, D.; Kim, M. R.; Kyu Song, J.; Kim, E.; Koo, J.; Kim, K. C.; Han, H.; Lee, Y.; Won Ahn, C., *ChemElectroChem* **2022,** *9* (1), e202101344.
90. Xiao, J.; Jin, Q.; Cang, R.; Gao, H.; Yao, J., *Electrochimica Acta* **2023,** *451*, 142289.
91. Xu, H.; Chen, G.; Du, F.; Wang, X.; Dall'Agnese, Y.; Gao, Y., *Journal of Physics D: Applied Physics* **2022,** *55* (20), 204002.
92. Zhang, W.; Pan, Z.-Z.; Lv, W.; Lv, R.; Shen, W.; Kang, F.; Yang, Q.-H.; Weng, Y.; Huang, Z.-H., *Carbon* **2019,** *153*, 625-633.
93. Jiang, R.; Yuan, H.; Wei, X.; Wang, H.; Shin, H.-J.; Lan, J.; Yu, Y.; Yang, X., *Materials Chemistry Frontiers* **2021,** *5* (23), 8218-8228.
94. Yang, J.; Bao, W.; Jaumaux, P.; Zhang, S.; Wang, C.; Wang, G., *Advanced Materials Interfaces* **2019,** *6* (8), 1802004.
95. Ampong, D. N.; Agyekum, E.; Agyemang, F. O.; Mensah-Darkwa, K.; Andrews, A.; Kumar, A.; Gupta, R. K., *Discover Nano* **2023,** *18* (1), 3.
96. Khan, M. U.; Du, L.; Fu, S.; Wan, D.; Bao, Y.; Feng, Q.; Grasso, S.; Hu, C., *Coatings* **2022,** *12* (4), 516.
97. Guo, Y.; Zhang, D.; Yang, Y.; Wang, Y.; Bai, Z.; Chu, P. K.; Luo, Y., *Nanoscale* **2021,** *13* (8), 4624-4633.
98. Guo, Y.; Zhang, D.; Bai, Z.; Yang, Y.; Wang, Y.; Cheng, J.; Chu, P. K.; Luo, Y., *Dalton Transactions* **2022,** *51* (4), 1423-1433.
99. Nahirniak, S.; Ray, A.; Saruhan, B., *Batteries* **2023,** *9* (2), 126.
100. Cheng, R.; Hu, T.; Zhang, H.; Wang, C.; Hu, M.; Yang, J.; Cui, C.; Guang, T.; Li, C.; Shi, C., *The Journal of Physical Chemistry C* **2018,** *123* (2), 1099-1109.
101. Wang, Z.; Cao, D.; Ren, M.; Zhang, H.; Pan, L.; Zhang, C. J.; Yang, J., *Journal of Alloys and Compounds* **2022,** *892*, 162037.
102. Jiang, T.; Xiong, Q.; Yang, H.; Chen, G. Z., *Journal of Physics: Energy* **2023**.
103. Bai, W.; Tang, H.; Zhai, J.; Cui, C.; Wang, W.; Cheng, C.; Ren, E.; Xiao, H.; Zhou, M.; Guo, R., *Industrial & Engineering Chemistry Research* **2022,** *61* (34), 12555-12566.
104. Likitaporn, C.; Okhawilai, M.; Kasemsiri, P.; Qin, J.; Potiyaraj, P.; Uyama, H., *Scientific Reports* **2022,** *12* (1), 19915. DOI 10.1038/s41598-022-24578-8.
105. Jiang, R.; Yuan, H.; Wei, X.; Wang, H.; Shin, H.-J.; Lan, J.; Yu, Y.; Yang, X., *Materials Chemistry Frontiers* **2021,** *5* (23), 8218-8228. DOI 10.1039/D1QM00823D.
106. Hu, Z.; Xie, Y.; Yu, D.; Liu, Q.; Zhou, L.; Zhang, K.; Li, P.; Hu, F.; Li, L.; Chou, S.; Peng, S., *ACS Nano* **2021,** *15* (5), 8407-8417. DOI 10.1021/acsnano.0c10558.
107. Guo, Y.; Zhang, D.; Bai, Z.; Yang, Y.; Wang, Y.; Cheng, J.; Chu, P. K.; Luo, Y., *Dalton Transactions* **2022,** *51* (4), 1423-1433. DOI 10.1039/D1DT03718H.
108. Zhou, Z.; Panatdasirisuk, W.; Mathis, T. S.; Anasori, B.; Lu, C.; Zhang, X.; Liao, Z.; Gogotsi, Y.; Yang, S., *Nanoscale* **2018,** *10* (13), 6005-6013. DOI 10.1039/C8NR00313K.
109. Xie, L.; Bi, J.; Xing, Z.; Gao, X.; Meng, L.; Liu, C., *Journal of Power Sources* **2022,** *547*, 232011. DOI https://doi.org/10.1016/j.jpowsour.2022.232011.

110. Zhang, S.; Chen, M.; Zhao, X.; Cai, J.; Yan, W.; Yen, J. C.; Chen, S.; Yu, Y.; Zhang, J., *Electrochemical Energy Reviews* **2021,** *4*, 336-381.
111. Zhao, S.; Wang, R.; Tian, T.; Liu, H.; Zhang, H.; Tang, H., *ACS Sustainable Chemistry & Engineering* **2022,** *10* (13), 4269-4278.
112. Hu, X.; Qin, J.; Wang, Y.; Wang, J.; Yang, A.; Tsang, Y. F.; Liu, B., *Journal of Colloid and Interface Science* **2022,** *628*, 327-337.
113. Tahir, K.; Miran, W.; Jang, J.; Maile, N.; Shahzad, A.; Moztahida, M.; Ghani, A. A.; Kim, B.; Jeon, H.; Lim, S.-R., *Chemosphere* **2021,** *268*, 128784.
114. Liu, D.; Wang, R.; Chang, W.; Zhang, L.; Peng, B.; Li, H.; Liu, S.; Yan, M.; Guo, C., *Journal of Materials Chemistry A* **2018,** *6* (42), 20887-20895.
115. Fei, M.; Lin, R.; Deng, Y.; Xian, H.; Bian, R.; Zhang, X.; Cheng, J.; Xu, C.; Cai, D., *Nanotechnology* **2017,** *29* (3), 035403.
116. Lopez, M.; Morales-Garcia, A.; Vines, F.; Illas, F., *ACS Catalysis* **2021,** *11* (21), 12850-12857.
117. Morales-Garcia, A.; Calle-Vallejo, F.; Illas, F., *ACS Catalysis* **2020,** *10* (22), 13487-13503.
118. Liu, D.; Wang, R.; Chang, W.; Zhang, L.; Peng, B.; Li, H.; Liu, S.; Yan, M.; Guo, C., *Journal of Materials Chemistry A* **2018,** *6* (42), 20887-20895. DOI 10.1039/C8TA07305H.
119. Ranjith, K. S.; Vilian, A. E.; Ghoreishian, S. M.; Umapathi, R.; Huh, Y. S.; Han, Y.-K., *Sensors and Actuators B: Chemical* **2021,** *344*, 130202.
120. Al-Dhahebi, A. M.; Jose, R.; Mustapha, M.; Saheed, M. S. M., *Food Chemistry* **2022,** *390*, 133105.
121. Wang, S.; Shao, H.-Q.; Liu, Y.; Tang, C.-Y.; Zhao, X.; Ke, K.; Bao, R.-Y.; Yang, M.-B.; Yang, W., *Composites Science and Technology* **2021,** *202*, 108600.
122. Sharifuzzaman, M.; Zahed, M. A.; Reza, M. S.; Asaduzzaman, M.; Jeong, S.; Song, H.; Kim, D. K.; Zhang, S.; Park, J. Y., *Advanced Functional Materials* **2023**, 2208894.
123. Ranjith, K. S.; Vilian, A. E.; Ghoreishian, S. M.; Umapathi, R.; Hwang, S.-K.; Oh, C. W.; Huh, Y. S.; Han, Y.-K., *Journal of Hazardous Materials* **2022,** *421*, 126775.
124. Chen, W.; Zhang, D.; Yang, K.; Luo, M.; Yang, P.; Zhou, X., *Chemical Engineering Journal* **2021,** *413*, 127524. DOI https://doi.org/10.1016/j.cej.2020.127524.
125. Singh, M.; Gupta, A.; Sundriyal, S.; Dubey, P.; Jain, K.; Dhakate, S., *Journal of Energy Storage* **2022,** *49*, 104193.
126. Gupta, A.; Gurunathan, P.; Ramesha, K.; Singh, M.; Dhakate, S. R., *Energy Storage* **2019**.
127. Lokhande, P. E.; Chavan, U. S.; Pandey, A., *Electrochemical Energy Reviews* **2020,** *3* (1), 155-186. DOI 10.1007/s41918-019-00057-z.
128. Zhang, J.; Seyedin, S.; Gu, Z.; Yang, W.; Wang, X.; Razal, J. M., *Nanoscale* **2017,** *9* (47), 18604-18608.
129. Seyedin, S.; Yanza, E. R. S.; Razal, J. M., *Journal of Materials Chemistry A* **2017,** *5* (46), 24076-24082.
130. Hwang, H.; Byun, S.; Yuk, S.; Kim, S.; Song, S. H.; Lee, D., *Applied Surface Science* **2021,** *556*, 149710.
131. Yan, S.-x.; Luo, S.-h.; Wang, Q.; Zhang, Y.-h.; Liu, X., *Composites Part B: Engineering* **2021,** *224*, 109246. DOI https://doi.org/10.1016/j.compositesb.2021.109246.
132. Kshetri, T.; Khumujam, D. D.; Singh, T. I.; Lee, Y. S.; Kim, N. H.; Lee, J. H., *Chemical Engineering Journal* **2022,** *437*, 135338. DOI https://doi.org/10.1016/j.cej.2022.135338.
133. Pathak, I.; Acharya, D.; Chhetri, K.; Lohani, P. C.; Subedi, S.; Muthurasu, A.; Kim, T.; Ko, T. H.; Dahal, B.; Kim, H. Y., *Journal of Materials Chemistry A* **2023,** *11* (10), 5001-5014.
134. Pathak, I.; Acharya, D.; Chhetri, K.; Chandra Lohani, P.; Subedi, S.; Muthurasu, A.; Kim, T.; Ko, T. H.; Dahal, B.; Kim, H. Y., *Journal of Materials Chemistry A* **2023,** *11* (10), 5001-5014. DOI 10.1039/D2TA09726E.
135. Donthula, K.; Vooradi, R.; Patnaikuni, V. S.; Kakunuri, M., *Journal of The Electrochemical Society* **2023,** *170* (3), 030508.

136. Khumujam, D. D.; Kshetri, T.; Singh, T. I.; Kim, N. H.; Lee, J. H., *Chemical Engineering Journal* **2022,** *449*, 137732. DOI https://doi.org/10.1016/j.cej.2022.137732.
137. Tao, X.; Zhang, L.; He, X.; Fang, L.; Wang, H.; Zhang, L.; Yu, L.; Zhu, G., *Molecules* **2022,** *27* (15), 4890.
138. Wang, J.; Huang, Y.; Zhang, S.; Du, X.; Duan, Z.; Sun, X., *Journal of Materials Science & Technology* **2023,** *147*, 112-123. DOI https://doi.org/10.1016/j.jmst.2022.10.071.
139. Pathak, I.; Acharya, D.; Chhetri, K.; Chandra Lohani, P.; Hoon Ko, T.; Muthurasu, A.; Subedi, S.; Kim, T.; Saidin, S.; Dahal, B.; Yong Kim, H., *Chemical Engineering Journal* **2023,** *469*, 143388. DOI https://doi.org/10.1016/j.cej.2023.143388.
140. Zhou, G.; Wang, X.; Wan, T.; Liu, C.; Chen, W.; Jiang, S.; Han, J.; Yan, Y.; Li, M. C.; Mei, C., *Energy & Environmental Materials* **2022**, e12454.
141. Chen, B.; Song, Q.; Zhou, Z.; Lu, C., *Advanced Materials Interfaces* **2021,** *8* (12), 2002168.
142. Hwang, H.; Yang, S.; Yuk, S.; Lee, K.-S.; Byun, S.; Lee, D., *NPG Asia Materials* **2023,** *15* (1), 29. DOI 10.1038/s41427-023-00476-x.

WILEY-VCH

Table of Content Entry

Application Scopes of Miniaturized MXene-Functionalized Electrospun Nanofibers-Based Electrochemical Energy Devices

Sanaz Khademolqorani, Seyedeh Nooshin Banitaba, Ashish Gupta, Nazanin Poursharifi, Ali Akbar Ghaffari, Vijaykumar V. Jadhav*, Waqas Ul Arifeen*, Mandeep Singh, Munu Borah, Elham Chamanehpour, Yogendra Kumar Mishra**

Keywords: Electrospun fibers, Battery, Fuel cell, Biosensor, Supercapacitor, Actuators.

Combinatorial materials in form of electrospun nanofibers exhibit enormous potential towards advancing the performance of electrochemical devices. This review briefly presents the synthesis of MXene based composite nanofibers by electrospinning technique and their potential applications in energy technologies. MXene based engineering of nanofibers via electrospinning and corresponding properties are the main focus in milieu of sensing and energy technologies.

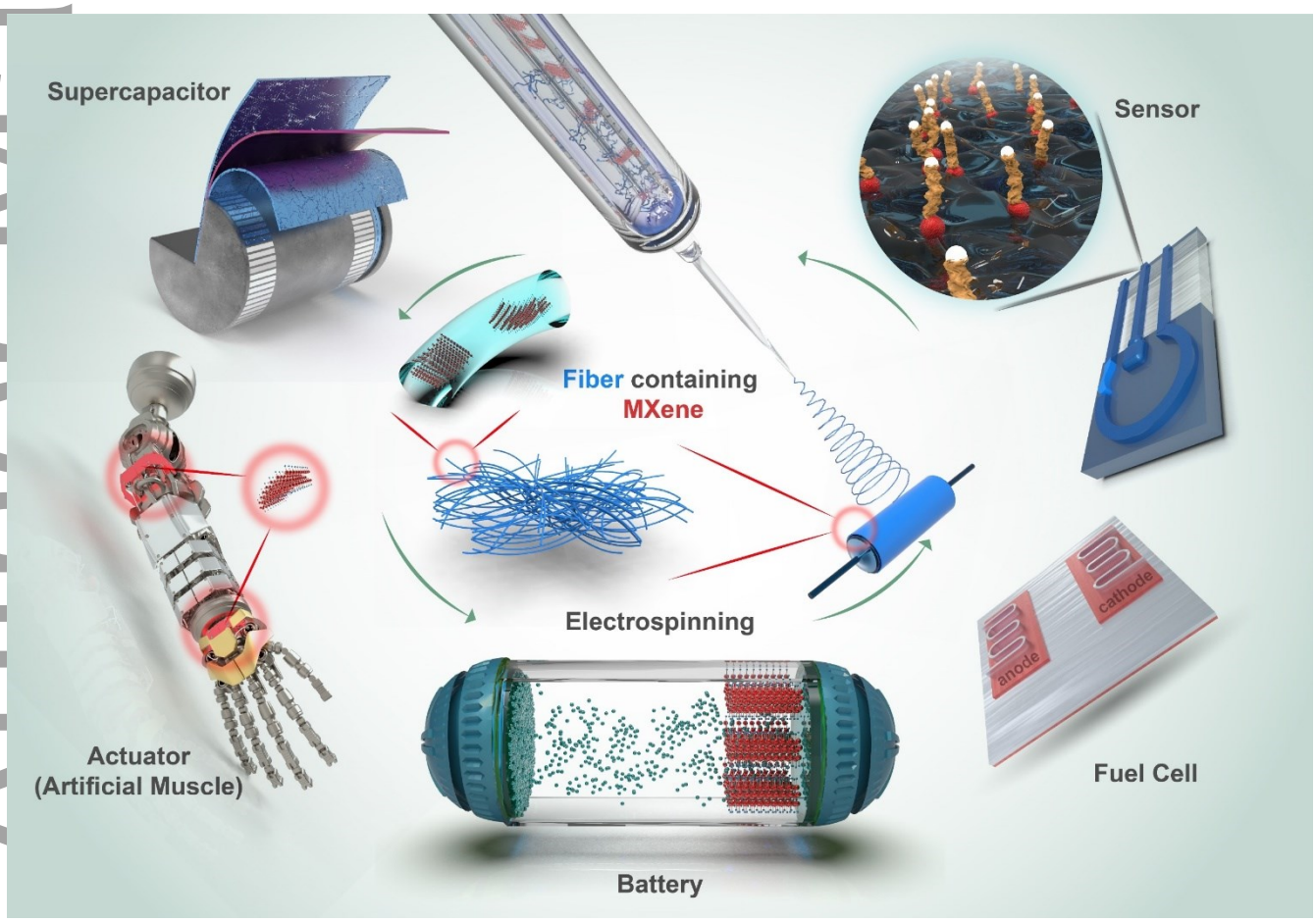

Author Biographies

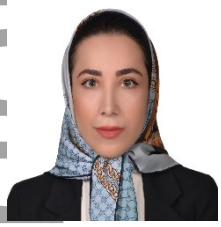

Banitaba, Ph. D. in Textile Engineering, has recently graduated from the Postdoctoral level at Amirkabir University of Technology. She has over ten years of research experience in the field of fabricating and analyzing electrospun nanostructures. Her main research interests are the design and development of solvent-free electrospun electrolytes incorporating active and inert materials to synthesize all-solid-state and flexible LIBs. Currently, she is active in research and development in her private laboratory. Dr. Banitaba has authored over 30 peer-reviewed scientific publications with 400 citations.

Khademolqorani is a highly accomplished Ph.D. researcher with experience working on several academic research projects at the Isfahan University of Technology and Denmark technical university. Her research has focused on fabrication, from conventional constructions to nanostructures, as well as fabricating innovative architectures for multiple fields, all applied across a wide range of research, development, and optimization. Dr. Khademolqorani hitherto has authored over 10 scientific publications. She currently leads a private laboratory where she continues to explore new and innovative approaches to her field.

Yogendra Kumar Mishra is Professor MSO at the Mads Clausen Institute, University of Southern Denmark, Sønderborg. Previously, he was leading a group at the Kiel University, Germany. He did Habilitation (Materials Science, 2015) from Kiel University and Ph.D. (Physics, 2008) from JNU, New Delhi, India. He is Humboldtian and recently awarded with Fellow of Royal Society of Chemistry, UK. He introduced the flame process for tetrapod nanostructuring and its 3D networks which found many applications in different technologies including using them as novel templates new 3D nanomaterials engineering. Smart Materials Lab is developing tetrapod-based spongy materials for advanced technologies.